Available online at www.worldscientificnews.com

World Scientific News

An International Scientific Journal

WSN 143 (2020) 224-261 EISSN 2392-2192

Force Modeling and Dynamic Behaviour of Multi-Dimensional Vibration Assisted Micro-End Milling: Linear and Nonlinear Analyses

M. G. Sobamowo*, S. J. Ojolo, O. K. Olawale, O. A. Adesina

Department of Mechanical Engineering, University of Lagos, Akoka, Lagos State, Nigeria

*E-mail address: mikegbeminiyi@gmail.com

ABSTRACT

The concept of component miniaturization is core in the production of sensitive components of the micro, nano and meso-scale. Vibration assisted micro-end milling is a miniaturized machining method that effectively produce these components. This paper presents the linear and nonlinear models describing the vibratory behavior of the sensitive system bearing in mind the amplitude stability phenomenon. The linear case is considered and solved analytically, the non-linear case is solved using differential transform method. With the aid of the developed solutions, parametric studies are carried out and the results are discussed. It is hope that the present study will help the manufacturing industry's desire for maximizing metal removal rates while maintaining acceptable surface finish and tool life especially in the micro machining of various components for industrial applications, medical and energy industries.

***Keywords*:** Vibration assisted micro-milling, Multidimensional vibration, Dynamic analysis, Stability, Micro-milling

1. INTRODUCTION

Machining, as a process of transforming a component into finished product of geometrically predetermined shapes and forms, comes with the ultimate goal of maximizing

(Received 20 February 2020; Accepted 12 March 2020; Date of Publication 13 March 2020)

profit and reducing losses in the most efficient way possible. In such process, the concept of component miniaturization is core in the production of sensitive components of the micro, nano and meso-scale. Vibration assisted machining (VAM) is a miniaturized machining method that engages a periodically controlled vibration with a small amplitude forced on the workpiece or the cutting tool. This type of machining improves the machining process by enhancing the material removal rate, surface finish, tool wear, a tool life and the overall surface finish. In fact, the engineering of producing quality delicate part at micro scale especially in the field of aerospace and telecommunication has brought micro milling as one of the new frontiers in the machining process. The application of the vibration assisted machining to the micro-machining gives a type of machining process called Vibration assisted micro-machining. However, the dynamic behaviour and the stability of such machining process have aroused the interests to various researchers. Consequently, a number of research works has been presented on the type of machining process. Xiao et al [1] performed time-domain simulation for cutting stability in convectional machining (CM) and vibration-assisted machining (VAM) giving force and vibration levels for selected cutting conditions. The result showed that VAM can suppress chatter and increase cutting stability under the selected cutting conditions regardless of the tool geometry. Few years later, Tabatabaei et al [2] applied the conventional frequency domain method to obtain the stability lobe diagram (SLD) for vibration-assisted machining (VAM).

The approach adopted in their work cannot be used to analyze the effect of vibration frequency on cutting stability.

The cutting process dynamics has an important part in the study of the various characteristics of the machining processes such as the positioning accuracy of the cutting tool with respect to the workpiece, the roughness of the machined surface, dynamic stability and geometrical error of the machined component. Therefore, Bao and Tansel [3] submitted analytical cutting force model for the micro-end-milling operations. In the work, the differences in the tool tip trajectory between micro end milling and the conventional end milling was considered. A year later, Fan and Miller [4] presented force modeling in vibration assisted cutting while in the same year, Dow et al. [5] a vibration assisted machining using elliptical tool motion was studied. Hanna and Tobias [6] carried out a study on face-milling and turning processes, where both cutting force non-linearities and structural non-linearities are considered. Altintas and Budak [7] presented detailed analysis on the stability of the machining processes. Budak and Altintas [8, 9] submitted an analytical prediction of chatter stability. Luo et al. [10] investigated the appearance of the dynamic instabilities especially chatter phenomena. It was concluded in these research works that vibration assisted machining applied to the conventional milling improves the overall cutting performances of micro milling.

A multi-dimensional vibration assisted micromachining was introduced in the late 1990s. This type of machining has been proven to be very efficient as it leads to reductions in the tool force [11, 12], improves machining accuracy [13, 14], and prolongs tool life [15] compared to the one-dimensional vibration assisted micro-milling Also, the multi-dimensional vibration assisted micromachining increases surface roughness, reduces tool wear, improved machining efficiency, surface quality and the tool life. This makes two-dimensional vibration assisted micro end milling an effective method of machining compared to the conventional way of machining [16-19]. Major setbacks of the electro discharge machining (EDM) which leads to increased production time and cost [20-27] and in conventional micro-milling such as the unpredicted tool life, premature failure of the micro tools, raid deterioration of the cutting-edge radius [25-28] have the overcome by the multi-dimensional vibration assisted micromachining.

Quite a few research works have been carried on the multi-dimensional vibration assisted micro end milling some of which are channeled into cutting parameters effects, validation and evaluation. Moreover, the milling processes involves more of complexity and therefore various research works in this field are often are tailored into studying the effect of cutting parameters or the external forcing functions on the system while stating assumptions to reduce the complexity involved. In such limit number of studies, Chen et al. [29] carried out experimental investigation on two-dimensional vibration assisted micro milling. The experiment revealed the micro milling process improves the machining accuracy and the surface roughness and prolongs the tool life. Due to better machining conditions and a reduction in the cutting forces. Kang et al. [30] developed a mechanistic model of cutting force of micro end milling process, the model considered the tool-workpiece contact and cutting-edge radius. Zaman et al. [31] proposed a three-dimensional analytical cutting force model which calculates the theoretical chip area at any specific angular position of the tool cutting edge by considering the geometry of the cutting-edge path. Chern and Chang et al [32] submitted that the vibration-assisted micro end milling can improve the cutting conditions this leads to high machining accuracy, and reduction in tool wear. Ding et al [33], investigates the machinability improvement of the hardened tool steel (HRC 55 and HRC 58) using 2-Dimensional vibration assisted micro end milling studying the effects of vibration parameters on machining parameters but using a linear chip thickness variation. However, the linear theory of machining depicts that at a certain depth of cut vibration becomes uncontrollable as the amplitude grow proportionately but this is actually not so in practice as the whole process stabilizes itself over time.

Gao et al [34] compared the stability behavior of VAM with that of CM to gain better understanding of the chatter suppression effect of VAM.

The small size of the cutting tool in micro milling processes, system parameter variations are of utmost important in order and needs to be kept at preferred level to secure continuity of process operations. The changes in the variation in stress distribution along the shaft of a micro milling tool is higher when compared to what happens in the conventional milling. This is due to the fact that in micro milling the feed per tooth to tool radius ratio has to be higher than in conventional milling to maintain optimum productivity. Therefore, the cutting force analysis is of core importance when analyzing micro-milling processes [3]. In this work, three-dimensional cutting force models combined with non-linear machine dynamics (which account for amplitude stability of the vibration-assisted micro-milling are analyzed. The models predict the dynamic behavior in all axis of rotation, the chip thickness and the cutting forces in vibration assisted micro-end milling.

2. MODEL DEVELOPMENT FOR THE MACHINING PROCESSES

In this section, the cutting force and vibration models for the vibration assisted micro-end milling are developed.

2. 1. Force Model development

Consider the vibration assisted micro-end milling as shown in Fig. 1. A frictional force which acts at the tool-workpiece contact surface is set-up as a result of the sliding motion between the two surfaces.

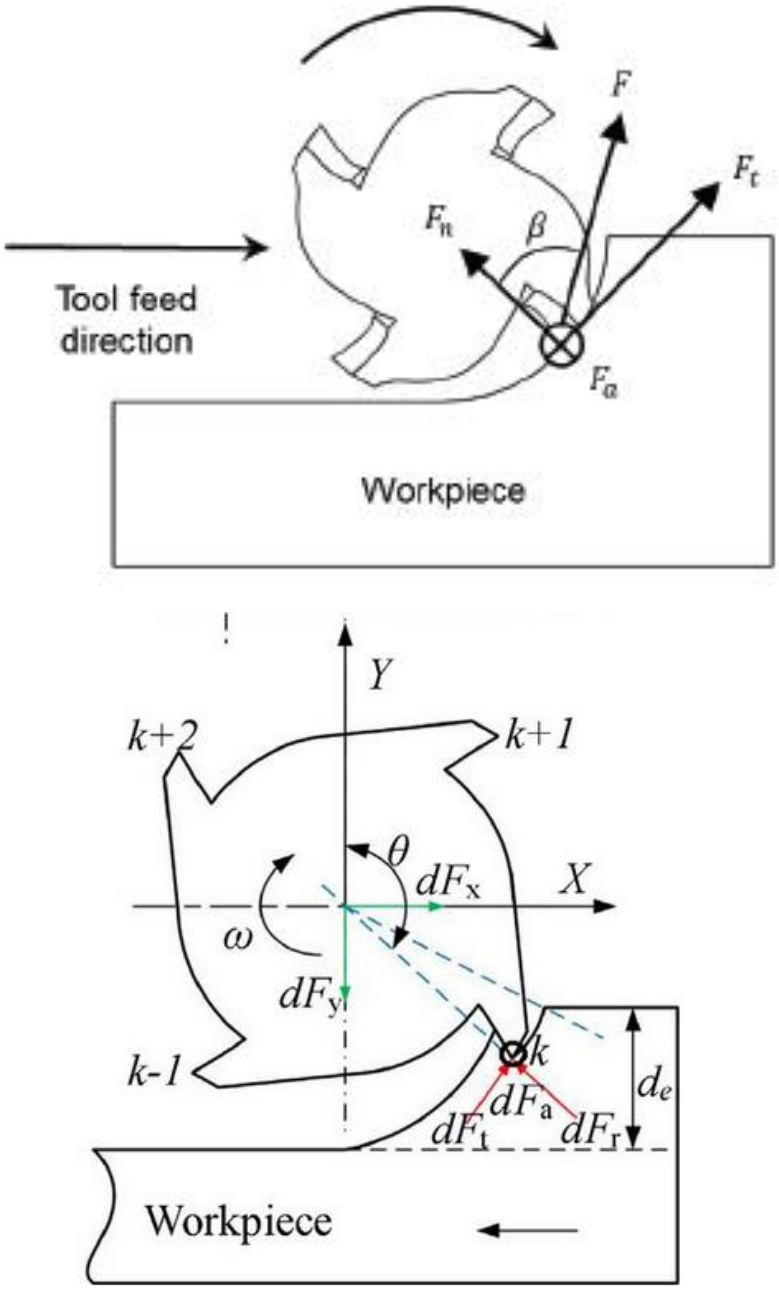

Fig. 1(a,b). Physical model of vibration assisted micro-end milling operation.

Provided elastic recovery takes place in the workpiece flank face, the horizontal and vertical component of the frictional force can be expressed as [32];

$$F_H = \frac{c_1 c_2 Y b R_e V_H}{\sqrt{3} E \sin(\theta_f)} \tag{1}$$

$$F_V = \frac{c_1 c_2 Yb R_e V_H}{E \sin(\theta_f)} \tag{2}$$

Considering only plane shear and the contact friction of the flank face of the micro cutting process. The normal component of the force and the friction acting on the shear plane can be expressed as;

$$N_S = \frac{\sigma \eta h}{\sin(\theta)} \tag{3}$$

$$F_S = \frac{\sigma \eta h}{\sqrt{3} \sin(\theta)} \tag{4}$$

Taking into consideration the tool edge radius, the principal cutting force and the tool edge radius can be expressed as,

$$F_C = F_S \cos(\phi) + N_S \sin(\phi) + F_H \tag{5}$$

$$F_T = -F_S \sin(\phi) + N_S \cos(\phi) + F_V \tag{6}$$

Integrating Eqs. (5) and (6) with respect to the tool angle, gives

$$\frac{dF_C}{d\theta} = \frac{\sigma f_t r \cos(\phi)}{\sqrt{3} \sin(\phi) \tan(\beta)} \sin(\theta) + \frac{\sigma f_t r}{\tan(\beta)} \sin(\theta) + \frac{c_1 R_e V_H \, \mathrm{Y} \, r}{\sqrt{3} E \sin(\theta_f) \tan(\beta)} \tag{7}$$

$$\frac{dF_T}{d\theta} = \frac{\sigma f_t r}{\sqrt{3} \tan(\beta)} \sin(\theta) + \frac{\sigma f_t r \cos(\phi)}{\sin(\phi) \tan(\beta)} \sin(\theta) + \frac{c_1 R_e V_H \, \mathrm{Y} \, r}{E \sin(\theta_f) \tan(\beta)} \tag{8}$$

The corresponding principal cutting force and thrusting force are obtained as

$$F_C = \frac{\sigma f_t r \cos(\phi)}{\sqrt{3} \sin(\phi) \tan(\beta)} + \frac{\sigma f_t r}{\tan(\beta)} + \frac{c_1 R_e V_H \, \mathrm{Y} \, r}{\sqrt{3} E \sin(\theta_f) \tan(\beta)} \tag{9}$$

$$F_T = \frac{\sigma f_t r}{\sqrt{3} \tan(\beta)} + \frac{\sigma f_t r \cos(\phi)}{\sin(\phi) \tan(\beta)} + \frac{c_1 R_e V_H \, \mathrm{Y} \, r}{E \sin(\theta_f) \tan(\beta)} \tag{10}$$

The axial component of the cutting force for micro end milling is the vertical component of the principal cutting force and can be written as

$$\mathrm{F}_A = \left(\frac{\sigma f_t r \cos(\phi)}{\sqrt{3} \sin(\phi) \tan(\beta)} + \frac{\sigma f_t r}{\tan(\beta)} + \frac{c_1 R_e V_H \, \mathrm{Y} \, r}{\sqrt{3} E \sin(\theta_f) \tan(\beta)} \right) \cos\left(\frac{\pi}{2} - \beta \right) \tag{11}$$

The forces in *x*, *y* and *z* directions are given as

$$F_x = -F_T \cos(\theta) - F_C \sin(\theta) \tag{12}$$

$$F_y = F_T \sin(\theta) - F_C \cos(\theta) \tag{13}$$

$$F_z = F_A \tag{14}$$

In Eq. (11), let

$$\eta = \frac{r}{\tan(\beta)}, \quad \beta_1 = \frac{\sigma\eta\cos(\phi)}{\sqrt{3}\sin(\phi)}, \quad \beta_2 = \sigma\eta, \quad \beta_3 = \frac{c_1 R_e V_H \eta \mathrm{Y}}{\sqrt{3}E\sin(\theta_f)} \tag{15}$$

where η = axial depth of cut while β_1, β_2, β_3 are the normal, shear and horizontal force approximations for computational ease and dexterity.

The 3-dimensional force model for the 2-dimensional micro end milling can written as

$$F_x = -\left(\beta_1 h + \beta_2 h + \beta_3\right)\cos(\theta) - \left(\frac{\beta_2 h}{\sqrt{3}} + \sqrt{3}\beta_1 h + \frac{\beta_3}{\sqrt{3}}\right)\sin(\theta) \tag{16}$$

$$F_y = \left(\beta_1 h + \beta_2 h + \beta_3\right)\sin(\theta) - \left(\frac{\beta_2 h}{\sqrt{3}} + \sqrt{3}\beta_1 h + \frac{\beta_3}{\sqrt{3}}\right)\cos(\theta) \tag{17}$$

$$F_z = -\left(\beta_1 h + \beta_2 h + \beta_3\right)\sin(\beta) - \left(\frac{\beta_2 h}{\sqrt{3}} + \sqrt{3}\beta_1 h + \frac{\beta_3}{\sqrt{3}}\right)\sin(\beta) \tag{18}$$

2. 2. Model development for the Linear Dynamic Behaviour

Consider the vibration of turning process represented as an excited mass-spring-damper system as shown in Figure 1. In the figure, the tool is compliant in *x* while the workpiece is assumed rigid. Taking into account the structural dynamics of the cutting zone, the vibration assisted micro end milling can be sufficiently model. A second-order forced spring-damper vibratory model in *x*, *y* and *z* directions is employed to represent the cutting tool and the workpiece system. Consider a homogeneous tool structural dynamic, therefore the vibratory system becomes

$$m_{tx}\ddot{x}_t + c_{tx}\dot{x}_t + k_{tx}x_t = F_x \tag{19}$$

$$m_{ty}\ddot{y}_t + c_{ty}\dot{y}_t + k_{ty}y_t = F_y \tag{20}$$

$$m_{tz}\ddot{z}_t + c_{tz}\dot{z}_t + k_{tz}z_t = F_z \tag{21}$$

while for the workpiece, the equations of motion are,

$$m_{wx}\ddot{x}_w + c_{wx}\dot{x}_w + k_{wx}x_w = F_{wx} \tag{22}$$

$$m_{wy}\ddot{y}_w + c_{wy}\dot{y}_w + k_{wy}y_w = F_{wy} \tag{23}$$

$$m_{wz}\ddot{z}_w + c_{wz}\dot{z}_w + k_{wz}z_w = F_{wz} \tag{24}$$

m, *c*, *k* and *F* represents the mass, the damper, the spring constants and the external forcing function on the vibration of the system, respectively.

The initial conditions are

$$t = 0, \quad x_t = x_e, \quad y_t = y_e, \; z_t = z_e \quad \frac{dx_t}{dt} = \frac{dy_t}{dt} = \frac{dz_t}{dt} = 0, \tag{25}$$

$$t = 0, \quad x_w = x_f, \quad y_w = y_f, \; z_w = z_f \quad \frac{dx_w}{dt} = \frac{dy_w}{dt} = \frac{dz_w}{dt} = 0, \tag{26}$$

The solutions of the displacement for non-periodic forces are

$$x_t(t) = \left[1 + \frac{F_x}{k_{tx}}\right] - \left[F_x + (x_e - 1)\right]\left\{\sqrt{1 + \frac{\left(\frac{c_{tx}}{2m_{tx}}\right)^2}{\left[\frac{k_{tx}}{m_{tx}} - \left(\frac{c_{tx}}{2m_{tx}}\right)^2\right]}}\, e^{\left(\frac{-c_{tx}}{2m_{tx}}\right)t} \sin\left[\left(\sqrt{\frac{k_{tx}}{m_{tx}} - \left(\frac{c_{tx}}{2m_{tx}}\right)^2}\right)t + \Phi_{d1}\right]\right\} + \frac{\left(\frac{c_{tx}}{m_{tx}}\right) e^{\left(\frac{-c_{tx}}{2m_{tx}}\right)t} \sin\left(\sqrt{\frac{k_{tx}}{m_{tx}} - \left(\frac{c_{tx}}{2m_{tx}}\right)^2}\right)t}{\sqrt{\frac{k_{tx}}{m_{tx}} - \left(\frac{c_{tx}}{2m_{tx}}\right)^2}} \tag{27}$$

$$y_t(t) = \left[1 + \frac{F_y}{k_{ty}}\right] - \left[F_y + (y_e - 1)\right]\left\{\sqrt{1 + \frac{\left(\frac{c_{ty}}{2m_{ty}}\right)^2}{\left[\frac{k_{ty}}{m_{ty}} - \left(\frac{c_{ty}}{2m_{ty}}\right)^2\right]}}\, e^{\left(\frac{-c_{ty}}{2m_{ty}}\right)t} \sin\left[\left(\sqrt{\frac{k_{ty}}{m_{ty}} - \left(\frac{c_{ty}}{2m_{ty}}\right)^2}\right)t + \Phi_{d2}\right]\right\} + \frac{\left(\frac{c_{ty}}{m_{ty}}\right) e^{\left(\frac{-c_{ty}}{2m_{ty}}\right)t} \sin\left(\sqrt{\frac{k_{ty}}{m_{ty}} - \left(\frac{c_{ty}}{2m_{ty}}\right)^2}\right)t}{\sqrt{\frac{k_{ty}}{m_{ty}} - \left(\frac{c_{ty}}{2m_{ty}}\right)^2}} \tag{28}$$

$$z_t(t) = \left[1 + \frac{F_z}{k_{tz}}\right] - \left[F_z + (z_e - 1)\right]\left\{\sqrt{1 + \frac{\left(\frac{c_{tz}}{2m_{tz}}\right)^2}{\left[\frac{k_{tz}}{m_{tz}} - \left(\frac{c_{tz}}{2m_{tz}}\right)^2\right]}}\, e^{\left(\frac{-c_{tz}}{2m_{tz}}\right)t} \sin\left[\left(\sqrt{\frac{k_{tz}}{m_{tz}} - \left(\frac{c_{tz}}{2m_{tz}}\right)^2}\right)t + \Phi_{d3}\right]\right\} + \frac{\left(\frac{c_{ty}}{m_{ty}}\right) e^{\left(\frac{-c_{tz}}{2m_{tz}}\right)t} \sin\left(\sqrt{\frac{k_{tz}}{m_{tz}} - \left(\frac{c_{tz}}{2m_{tz}}\right)^2}\right)t}{\sqrt{\frac{k_{tz}}{m_{tz}} - \left(\frac{c_{tz}}{2m_{tz}}\right)^2}} \tag{29}$$

where

$$\Phi_{d1} = tan^{-1}\left(\frac{\left[\frac{k_{tx}}{m_{tx}} - \left(\frac{c_{tx}}{2m_{tx}}\right)^2\right]}{\left(\frac{c_{tx}}{2m_{tx}}\right)}\right) \qquad \Phi_{d2} = tan^{-1}\left(\frac{\left[\frac{k_{ty}}{m_{ty}} - \left(\frac{c_{ty}}{2m_{ty}}\right)^2\right]}{\left(\frac{c_{ty}}{2m_{ty}}\right)}\right) \qquad \Phi_{d3} = tan^{-1}\left(\frac{\left[\frac{k_{tz}}{m_{tz}} - \left(\frac{c_{tz}}{2m_{tz}}\right)^2\right]}{\left(\frac{c_{tz}}{2m_{tz}}\right)}\right)$$

While for the workpiece, the solutions are

$$x_w(t)=\left[1+\frac{F_{wx}}{k_{wx}}\right]-\left[F_{wx}+\left(x_f-1\right)\right]\left\{\sqrt{1+\frac{\left(\frac{c_{wx}}{2m_{wx}}\right)^2}{\left[\frac{k_{wx}}{m_{wx}}-\left(\frac{c_{wx}}{2m_{wx}}\right)^2\right]}}e^{\left(\frac{-c_{wx}}{2m_{wx}}\right)t}\sin\left[\left(\sqrt{\frac{k_{wx}}{m_{wx}}-\left(\frac{c_{wx}}{2m_{wx}}\right)^2}\right)t+\Phi_{e1}\right]\right\}+\frac{\left(\frac{c_{wx}}{m_{wx}}\right)e^{\left(\frac{-c_{wx}}{2m_{wx}}\right)t}\sin\left(\sqrt{\frac{k_{wx}}{m_{wx}}-\left(\frac{c_{wx}}{2m_{wx}}\right)^2}\right)t}{\sqrt{\frac{k_{wx}}{m_{wx}}-\left(\frac{c_{wx}}{2m_{wx}}\right)^2}} \quad (30)$$

$$y_w(t)=\left[1+\frac{F_{yw}}{k_{wy}}\right]-\left[F_{yw}+\left(y_f-1\right)\right]\left\{\sqrt{1+\frac{\left(\frac{c_{wy}}{2m_{wy}}\right)^2}{\left[\frac{k_{wy}}{m_{wy}}-\left(\frac{c_{wy}}{2m_{wy}}\right)^2\right]}}e^{\left(\frac{-c_{wy}}{2m_{wy}}\right)t}\sin\left[\left(\sqrt{\frac{k_{wy}}{m_{wy}}-\left(\frac{c_{wy}}{2m_{wy}}\right)^2}\right)t+\Phi_{e2}\right]\right\}+\frac{\left(\frac{c_{wy}}{2m_{wy}}\right)e^{\left(\frac{-c_{wy}}{2m_{wy}}\right)t}\sin\left(\sqrt{\frac{k_{wy}}{m_{wy}}-\left(\frac{c_{wy}}{2m_{wy}}\right)^2}\right)t}{\sqrt{\frac{k_{wy}}{m_{wy}}-\left(\frac{c_{wy}}{2m_{wy}}\right)^2}} \quad (31)$$

$$z_w(t)=\left[1+\frac{F_{wz}}{k_{wz}}\right]-\left[F_{wz}+\left(z_f-1\right)\right]\left\{\sqrt{1+\frac{\left(\frac{c_{wz}}{2m_{wz}}\right)^2}{\left[\frac{k_{wz}}{m_{wz}}-\left(\frac{c_{wz}}{2m_{wz}}\right)^2\right]}}e^{\left(\frac{-c_{wz}}{2m_{wz}}\right)t}\sin\left[\left(\sqrt{\frac{k_{wz}}{m_{wz}}-\left(\frac{c_{wz}}{2m_{wz}}\right)^2}\right)t+\Phi_{e3}\right]\right\}+\frac{\left(\frac{c_{wz}}{m_{wz}}\right)e^{\left(\frac{-c_{wz}}{2m_{wz}}\right)t}\sin\left(\sqrt{\frac{k_{wz}}{m_{wz}}-\left(\frac{c_{wz}}{2m_{wz}}\right)^2}\right)t}{\sqrt{\frac{k_{wz}}{m_{wz}}-\left(\frac{c_{wz}}{2m_{wz}}\right)^2}} \quad (32)$$

where

$$\Phi_{e1}=tan^{-1}\left(\frac{\left[\frac{k_{wx}}{m_{wx}}-\left(\frac{c_{wx}}{2m_{wx}}\right)^2\right]}{\left(\frac{c_{wx}}{2m_{wx}}\right)}\right) \qquad \Phi_{e2}=tan^{-1}\left(\frac{\left[\frac{k_{wy}}{m_{wy}}-\left(\frac{c_{wy}}{2m_{wy}}\right)^2\right]}{\left(\frac{c_{wy}}{2m_{wy}}\right)}\right) \qquad \Phi_{e3}=tan^{-1}\left(\frac{\left[\frac{k_{wz}}{m_{wz}}-\left(\frac{c_{wz}}{2m_{wz}}\right)^2\right]}{\left(\frac{c_{wz}}{2m_{wz}}\right)}\right)$$

The relative dynamic displacement of the tool and the workpiece on all the three axis is obtained separately by the difference in the opposing vibrations along the same axis.

Therefore, the relative displacement in *X*, *Y* and *Z* becomes:

$$X=x_t-x_w \quad (33)$$

$$Y=y_t-y_w \quad (34)$$

$$Z=z_t-z_w \quad (35)$$

2. 3. Model development for the Non-Linear Dynamic Behaviour

Linear theory of machine tool chatter depicts that amplitude of vibration increases indefinitely once the depth of cut exceeds a critical level. Such description is not true with practice as the amplitude of vibration after an initial rapid increase undergoes stabilization by itself at a finite level. The amplitude stabilization in caused either by structural or the cutting process non-linearities. Therefore, the linear theory is incapable of explaining finite amplitude stability and as the same time cannot correctly depict the true vibrational behavior of the system

[6]. According to the work of Hannah [6] the damping coefficient is the hysteretic or structural damping and is giving as

$$c\dot{x}(t) = \frac{\vartheta}{\omega}\dot{x}(t) \tag{36}$$

The stiffness function is expressed as

$$k_x\left(\gamma_2 x^3 + \gamma_1 x^2 + x\right) \tag{37}$$

$$k_y\left(\gamma_2 y^3 + \gamma_1 y^2 + y\right) \tag{38}$$

$$k_z\left(\gamma_2 z^3 + \gamma_1 z^2 + z\right) \tag{39}$$

Considering structural non-linearities of the spindle dynamics, the novel non-linear machine tool dynamics combined with the force model then becomes;

$$m_{tx}\ddot{x}_t + \frac{\vartheta_{tx}}{\omega_{tx}}\dot{x}_t + k_{tx}\left(\gamma_2 x_t^3 + \gamma_1 x_t^2 + x_t\right) = F_x \tag{40}$$

$$m_{ty}\ddot{y}_t + \frac{\vartheta_{ty}}{\omega_{ty}}\dot{y}_{ty} + k_{ty}\left(\gamma_2 y_t^3 + \gamma_1 y_t^2 + y_t\right) = F_y \tag{41}$$

$$m_{tz}\ddot{z}_t + \frac{\vartheta_{tz}}{\omega_{tz}}\dot{z}_t + k_{tz}\left(\gamma_2 z_t^3 + \gamma_1 z_t^2 + z_t\right) = F_z \tag{42}$$

While the non-linear workpiece dynamics combined with the force model then becomes;

$$m_{wx}\ddot{x}_w + \frac{\vartheta_{wx}}{\omega_{wx}}\dot{x}_w + k_{wx}\left(\gamma_2 x_w^3 + \gamma_1 x_w^2 + x_w\right) = F_{wx} \tag{43}$$

$$m_{wy}\ddot{y}_w + \frac{\vartheta_{wy}}{\omega_{wy}}\dot{y}_{wy} + k_{wy}\left(\gamma_2 y_w^3 + \gamma_1 y_w^2 + y_w\right) = F_{wy} \tag{44}$$

$$m_{wz}\ddot{z}_w + \frac{\vartheta_{wz}}{\omega_{wz}}\dot{z}_w + k_{wz}\left(\gamma_2 z_w^3 + \gamma_1 z_w^2 + z_w\right) = F_{wz} \tag{45}$$

For example, the experimental constants in the nonlinear models for face milling are given by the work of Hannah and Tobias [35] as

$$\vartheta = 78250 \text{ Ib rad/in}, \quad \gamma_1 = 479.3 \text{ I/in}, \quad \gamma_2 = 264500 \text{ I/in}^2, \quad K = 1.87\ 10^6 \text{ Ib/in} \tag{46}$$

For this research work the values of constants used are assumed to be unity in case of micro-end milling as there are experiments to compute their values for the down-milling case.

2. 4. Chip Thickness Variation Models

The cutting force is significantly influenced by the uncut chip thickness. The calculation of cutting force in micro-end-milling is largely dependent on the accurate computation of the uncut chip thickness.

Li et al. [35] have shown that based on the true tooth paths, at a moment during the tool-workpiece engagement in milling, the uncut chip thickness for a cutter tooth engaged in cutting can be determined through finding the intersection point of the path curve left by the preceding tooth and the line passing through the current tooth tip as well as the cutter axis.

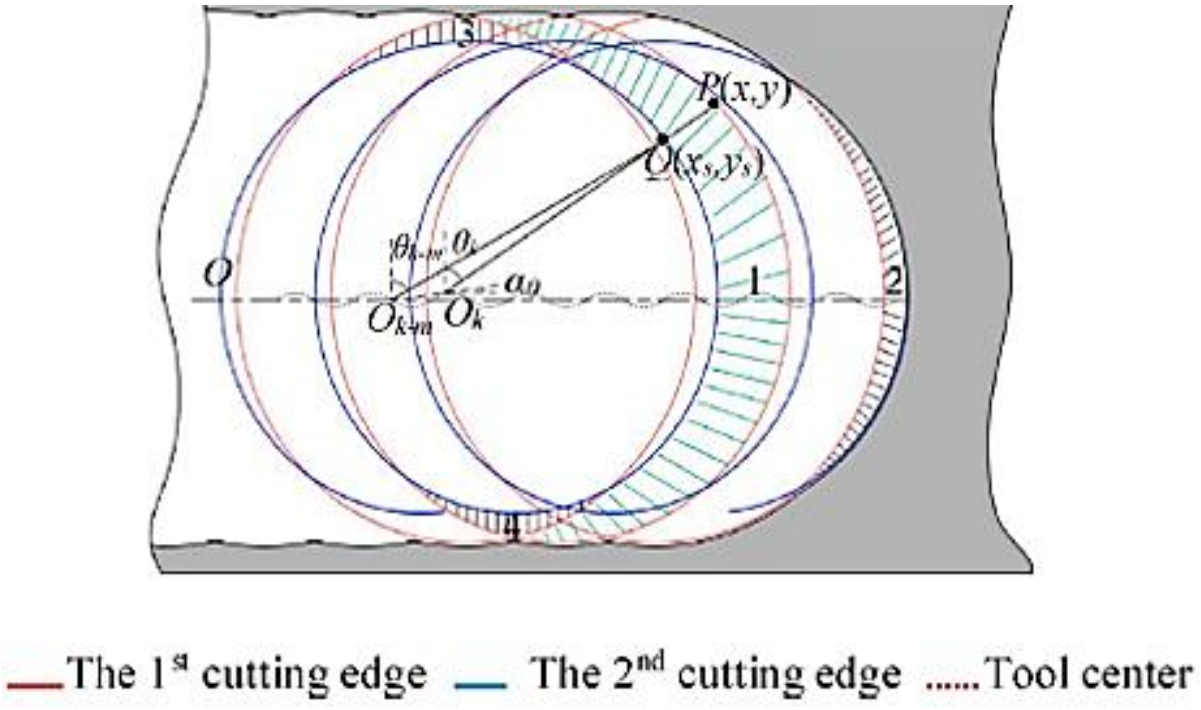

Fig. 2. The trochoidal trajectory of the tool tip for K = 2 micro-end operations [36].

According to the work of Tlusty and Macneil's model the chip thickness variation in a conventional milling can be expressed as [31]

$$h = f_z \sin(\theta) \tag{47}$$

In micro-milling with a large ratio of feed per tooth to tool radius, the actual uncut chip thickness is different from that of conventional milling. The work of Bao and Tansel [3] for more accurate chip thickness model for micro-end milling is expressed as

$$h = f_z \sin(\theta) - \frac{\mathbb{N}}{2\pi r} f_z^2 \sin(\theta)\cos(\theta) + \frac{1}{2f} f_z^2 \cos(\theta) \tag{48}$$

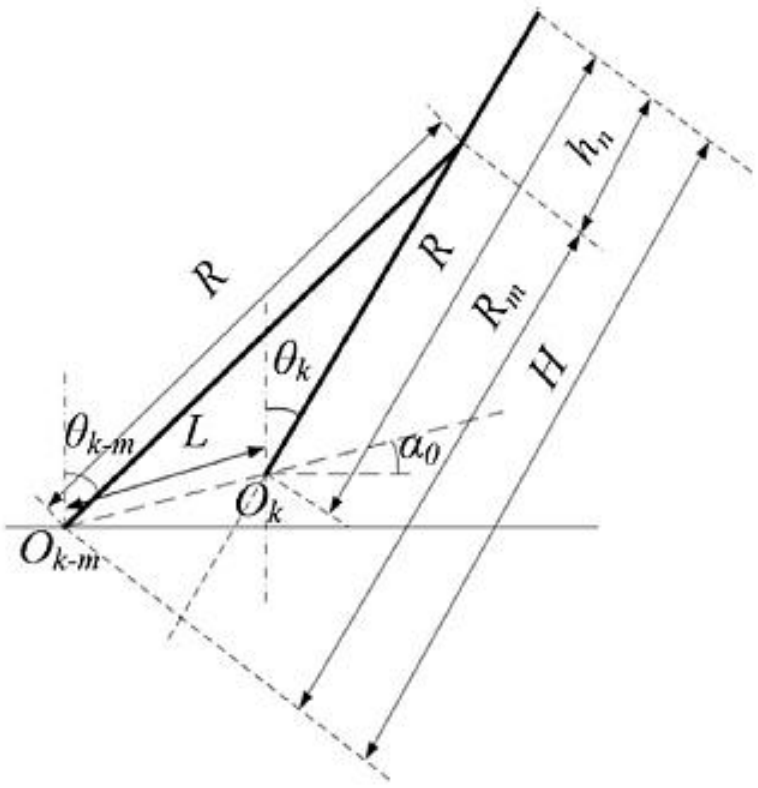

Fig. 3. The instantaneous uncut chip geometry calculations [35]

From geometrical relationship the instantaneous chip thickness with respect to the cutting tool tip is computed as

$$h_n = R + D\sin\left(\omega t - \frac{2\pi k}{\mathbb{N}} + \alpha\right) - \left(R^2 - D^2\left(\cos\left(\omega t - \frac{2\pi k}{\mathbb{N}} + \alpha\right)\right)^2\right)^{0.5} \tag{49}$$

where D is the distance between the tool centers of the respective tool tip which correspond to time t and S is given by;

$$\mathrm{D}=\sqrt{\left(\left(x(\mathrm{k},\mathrm{t})-\mathrm{x}(\mathrm{k}-1,s)\right)^2+\left(\left(\mathrm{y}(\mathrm{k},\mathrm{t})-y(\mathrm{k}-1,s)\right)^2\right)\right)} \tag{50}$$

3. METHOD OF SOLUTION FOR THE NONLINEAR DYNAMIC MODELS: DIFFERENTIAL TRANSFORM METHOD

In order to solve the developed non-linear models, recourse was made to an approximate analytical method, differential transform method. The basic definitions of the method are as

follows. If $u(x)$ is analytic in the domain T, then it will be differentiated continuously with respect to space *x*.

$$\frac{d^p u(x)}{dx^p} = \varphi(x, p) \text{ for } \quad \text{all } x \in T \tag{51}$$

for $x = x_i$, then $\varphi(x, p) = \varphi(x_i, p)$, where *p* belongs to the set of non-negative integers, denoted as the *p*-domain. Therefore eq. (52) can be rewritten as

$$U(p) = \varphi(x_i, p) = \left[\frac{d^p u(x)}{dt^p} \right]_{x=x_i} \tag{52}$$

where U_p is called the spectrum of $u(x)$ at $x = x_i$

If $u(x)$ can be expressed by Taylor's series, the $u(x)$ can be represented as

$$u(x) = \sum_p^{\infty} \left[\frac{(x - x_i)^p}{p!} \right] U(p) \tag{53}$$

where equ. (53) is called the inverse of $U(k)$ using the symbol 'D' denoting the differential transformation process and combining eq. (10) and eq. (12), it is obtained that

$$u(x) = \sum_{p=0}^{\infty} \left[\frac{(x - x_i)^p}{p!} \right] U(p) = D^{-1} U(p) \tag{54}$$

3. 1. Operational properties of differential transformation method

If $u(x)$ *and* $v(x)$ are two independent functions with space (x) where $U(p)$ and $V(p)$ are the transformed function corresponding to $u(x)$ and $v(x)$, then it can be proved from the fundamental mathematics operations performed by differential transformation that.

i. If $z(x) = u(x) \pm v(x)$, then $Z(p) = U(p) \pm V(p)$

ii. If $z(x) = \alpha u(x)$, then $Z(p) = \alpha U(p)$

iii. If $z(x) = \frac{du(x)}{dx}$, then $Z(p) = (p-1)\, U(p+1)$

iv. If $z(x) = u(x)v(x)$, then $Z(p) = \sum_{r=0}^{p} V(r) U(p-r)$

v. If $z(x) = u^m(x)$, then $Z(p) = \sum_{r=0}^{p} U^{m-1}(r) U(p-r)$

vi. If $z(x)=u(x)v(x)$, then $Z(p)=\sum_{r=0}^{p}(r+1)V(r+1)U(p-r)$

The application of differential transform method to the nonlinear problem is demonstrated in this section. The DTM recursive relations for the governing equation of motion (Eq. (1)) of the system is

$$m_{tx}(k+1)(k+2)X_t(k+2)+\frac{\vartheta_{tx}}{\omega_{tx}}(k+1)X_t(k+1)$$
$$+k_{tx}\left(\gamma_2\sum_{l=0}^{k}\sum_{p=0}^{k-l}X_t[l]X_t[p]X_t[k-l-p]+\gamma_1\sum_{l=0}^{k}X_t[l]X_t[k-l]+X_t(k)\right)=\Re_x(k) \quad (55)$$

$$m_{ty}(k+1)(k+2)Y_t(k+2)+\frac{\vartheta_{ty}}{\omega_{ty}}(k+1)Y_t(k+1)$$
$$+k_{ty}\left(\gamma_2\sum_{l=0}^{k}\sum_{p=0}^{k-l}Y_t[l]Y_t[p]Y_t[k-l-p]+\gamma_1\sum_{l=0}^{k}Y_t[l]Y_t[k-l]+Y_t(k)\right)=\Re_y(k) \quad (56)$$

$$m_{tz}(k+1)(k+2)Z_t(k+2)+\frac{\vartheta_{tz}}{\omega_{tz}}(k+1)Z_t(k+1)$$
$$+k_{tz}\left(\gamma_2\sum_{l=0}^{k}\sum_{p=0}^{k-l}Z_t[l]Z_t[p]Z_t[k-l-p]+\gamma_1\sum_{l=0}^{k}Z_t[l]Z_t[k-l]+Z_t(k)\right)=\Re_z(k) \quad (57)$$

For the workpiece, the DTM recursive relations for the governing equation of motions of the system are

$$m_{wx}(k+1)(k+2)X_w(k+2)+\frac{\vartheta_{wx}}{\omega_{wx}}(k+1)X_w(k+1)$$
$$+k_{wx}\left(\gamma_2\sum_{l=0}^{k}\sum_{p=0}^{k-l}X_w[l]X_w[p]X_w[k-l-p]+\gamma_1\sum_{l=0}^{k}X_w[l]X_w[k-l]+X_w(k)\right)=\Re_{wx}(k) \quad (58)$$

$$m_{wy}(k+1)(k+2)Y_w(k+2)+\frac{\vartheta_{wy}}{\omega_{wy}}(k+1)Y_w(k+1)$$
$$+k_{wy}\left(\gamma_2\sum_{l=0}^{k}\sum_{p=0}^{k-l}Y_w[l]Y_w[p]Y_w[k-l-p]+\gamma_1\sum_{l=0}^{k}Y_w[l]Y_w[k-l]+Y_w(k)\right)=\Re_{wy}(k) \quad (59)$$

$$m_{wz}(k+1)(k+2)Z_w(k+2)+\frac{\vartheta_{wz}}{\omega_{wz}}(k+1)Z_w(k+1)$$
$$+k_{wz}\left(\gamma_2\sum_{l=0}^{k}\sum_{p=0}^{k-l}Z_w[l]Z_w[p]Z_w[k-l-p]+\gamma_1\sum_{l=0}^{k}Z_w[l]Z_w[k-l]+Z_w(k)\right)=\Re_{wz}(k) \quad (60)$$

where $\Re(k)$ is the differential transform of the forcing function

The initial conditions in differential transforms are

$$X_t[0]=x_e,\quad Y_t[0]=y_e,\quad Z_t[0]=z_e\quad X_t[1]=0,\quad Y_t[1]=0,\quad Z_t[1]=0 \quad (61)$$

$$X_w[0]=x_f,\quad Y_w[0]=y_f,\quad Z_w[0]=z_f\quad X_w[1]=0,\quad Y_w[1]=0,\quad Z_w[1]=0 \quad (62)$$

The term by term analytical expressions for the solutions are too long to be included in this paper. Using the definition of DTM, the desired analytical solutions were established.

4. RESULTS AND DISCUSSION

The simulated results using the developed solutions are presented and discussed in this section. Also, parametric studies are carried out and discussed.

4. 1. Force Variations in the Feed Direction

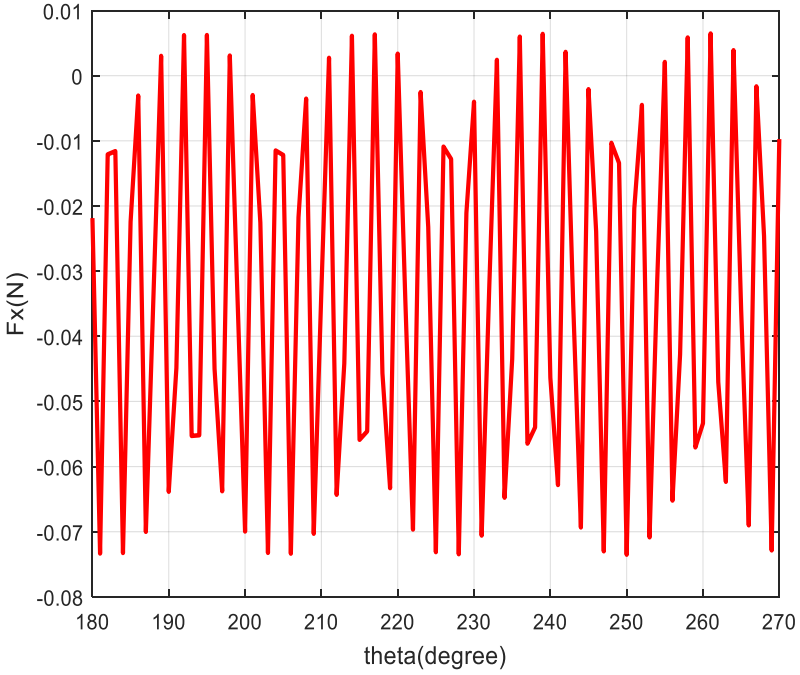

Fig. 4a. Force variation in feed direction for 0º - 90º

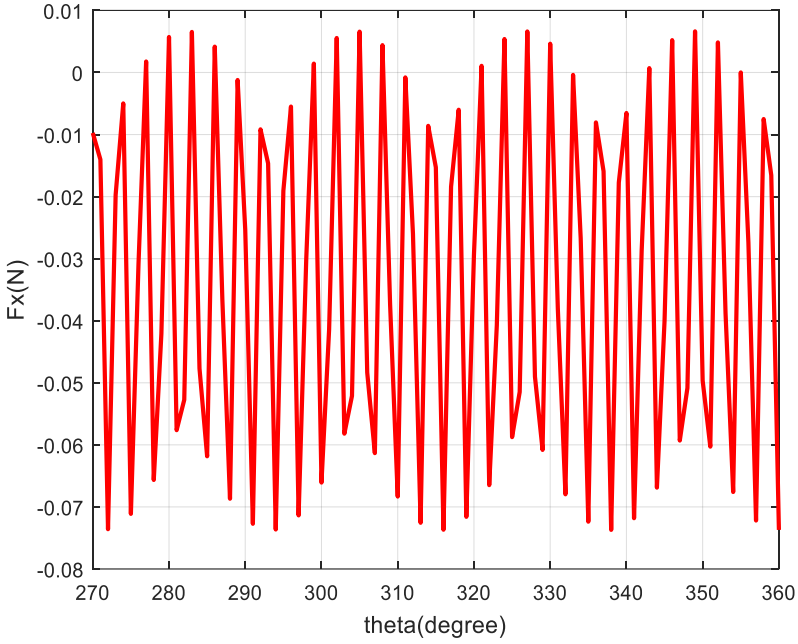

Fig. 4b. Force variation in feed direction for 90º - 180º

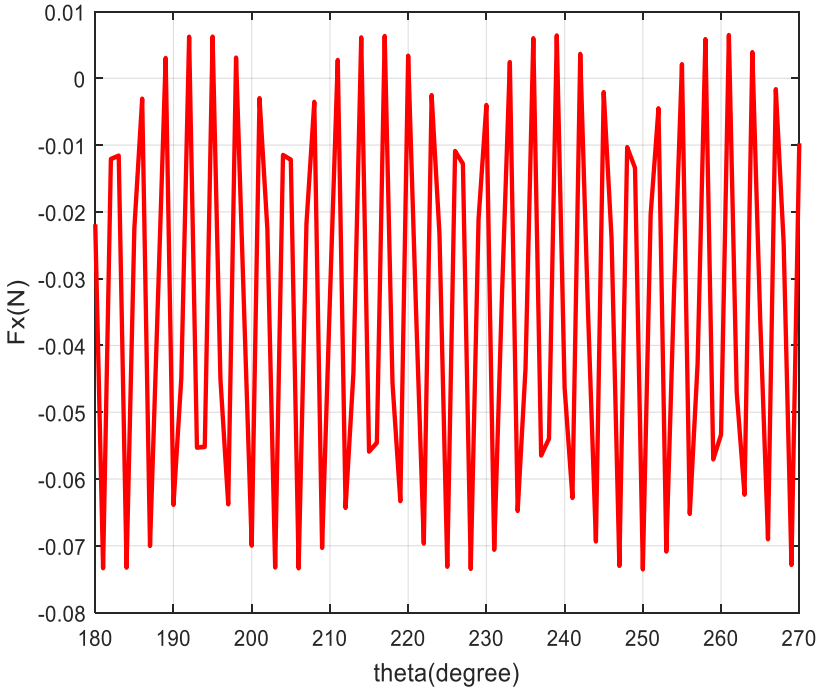

Fig. 4c. Force variation in feed direction for180º - 270º

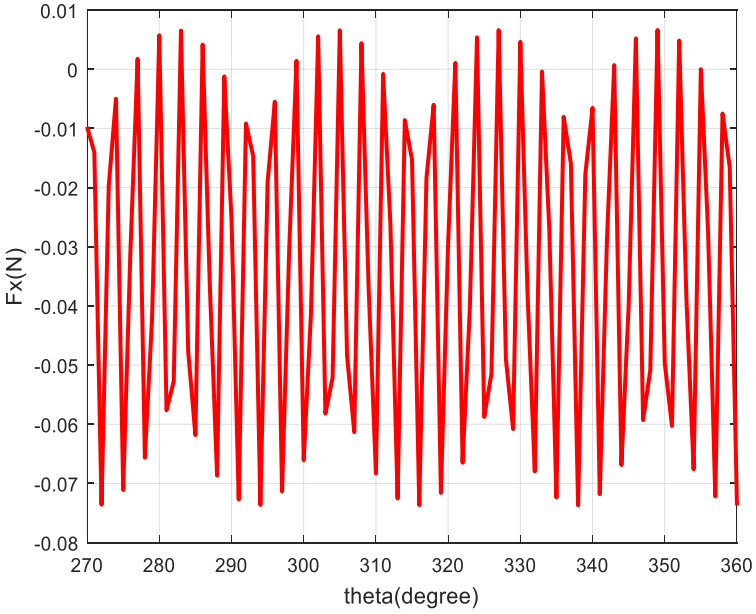

Fig. 4d. Force variation in feed direction for 270º - 360º

The force variation in the feed direction follows a sinusoidal function of repeated pattern. This shows that the cutter experiences the same magnitude of force in a cycle of cut as the tool direction changes.

4. 2. Force Variations in the Normal Direction

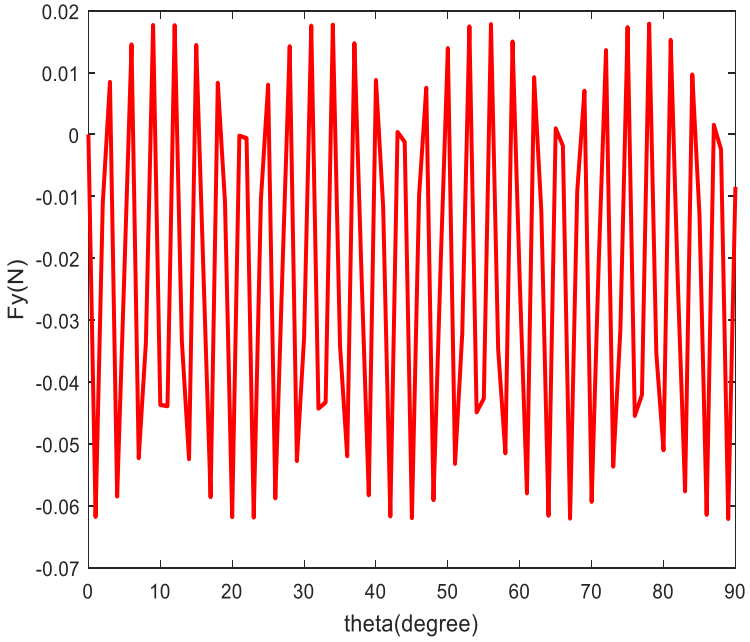

Fig. 5a. Force variation in normal direction for 0º - 90º

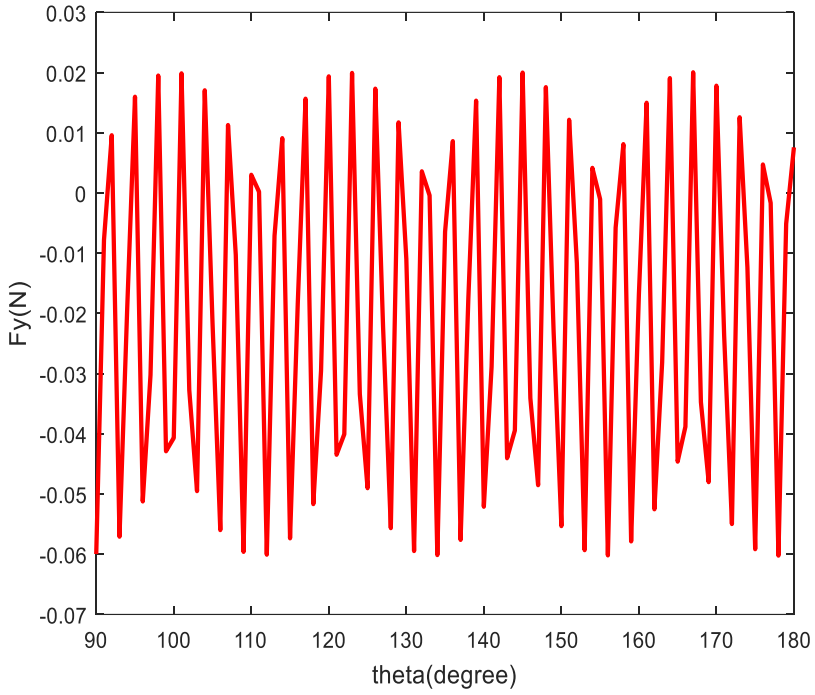

Fig. 5b. Force variation in normal direction for 90º - 180º

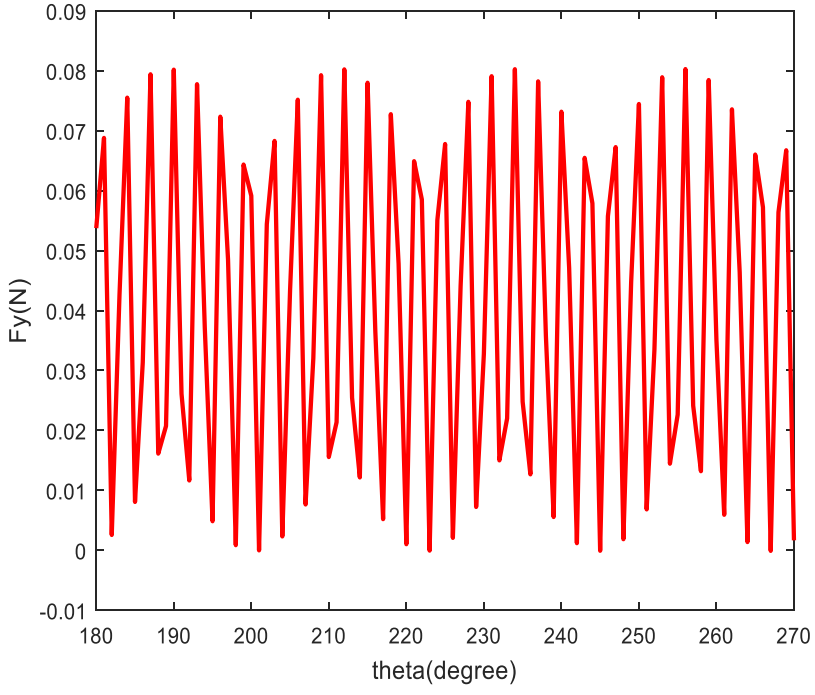

Fig. 5c. Force variation in normal direction for180º - 270º

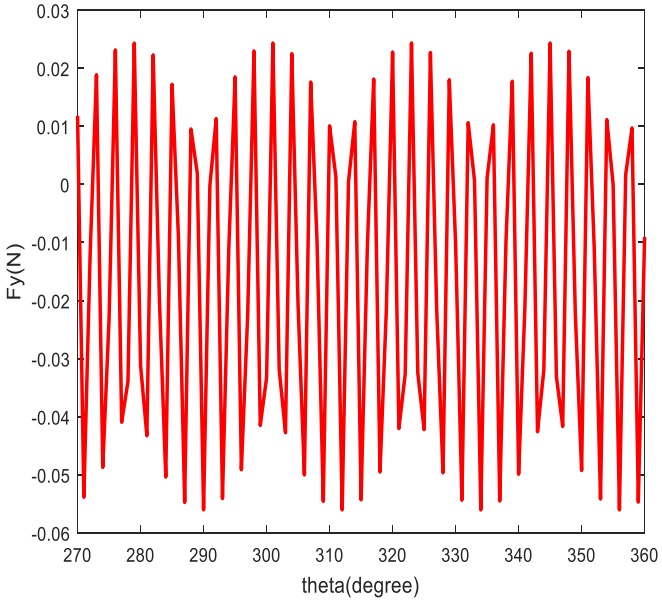

Fig. 5d. Force variation in normal direction for 270º - 360º

The force variation in the normal direction follows a sinusoidal function of repeated pattern but the cutter experience different changing magnitude of force in a cycle of cut as the tool direction changes, being maximum at 270º tool rotation angle and dropping back to a minimum level experienced at 180º. The force experienced here is selective of the angle of rotation.

4. 3. Force Variations in the Axial Direction

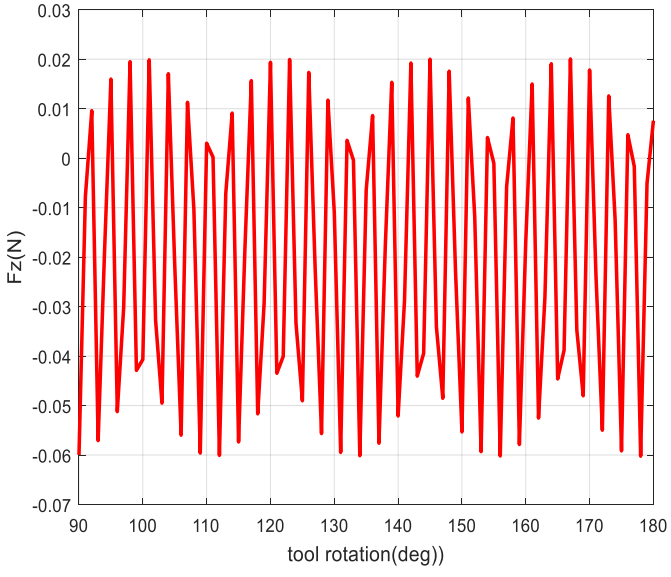

Fig. 6a. Force variation in axial direction for 0º - 90º

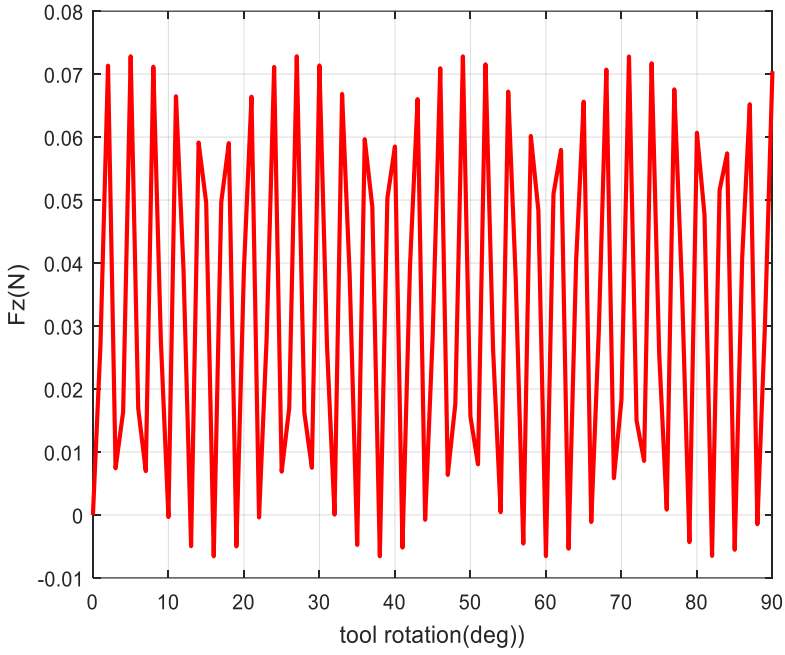

Fig. 6b. Force variation in axial direction for 90º - 180º

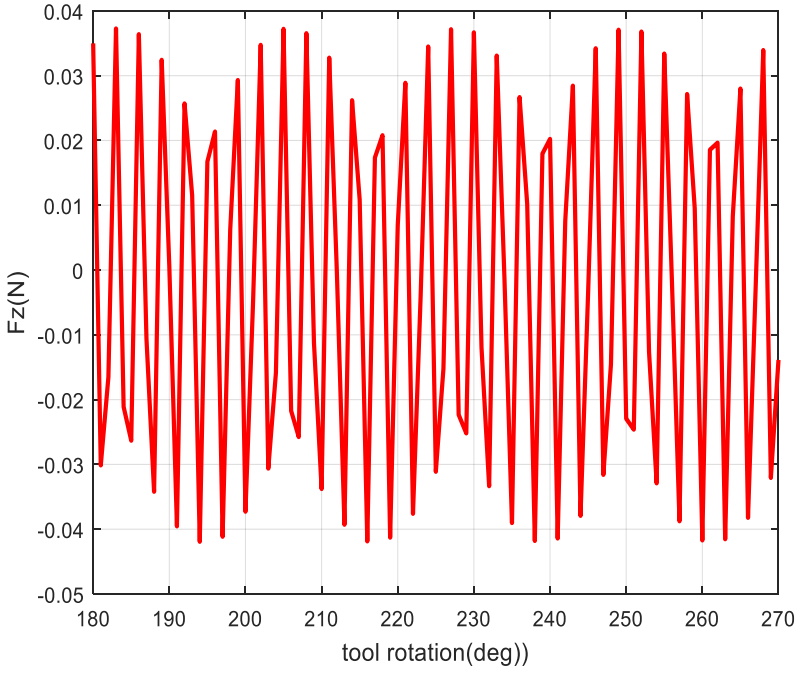

Fig. 6c. Force variation in axial direction for180º - 270º

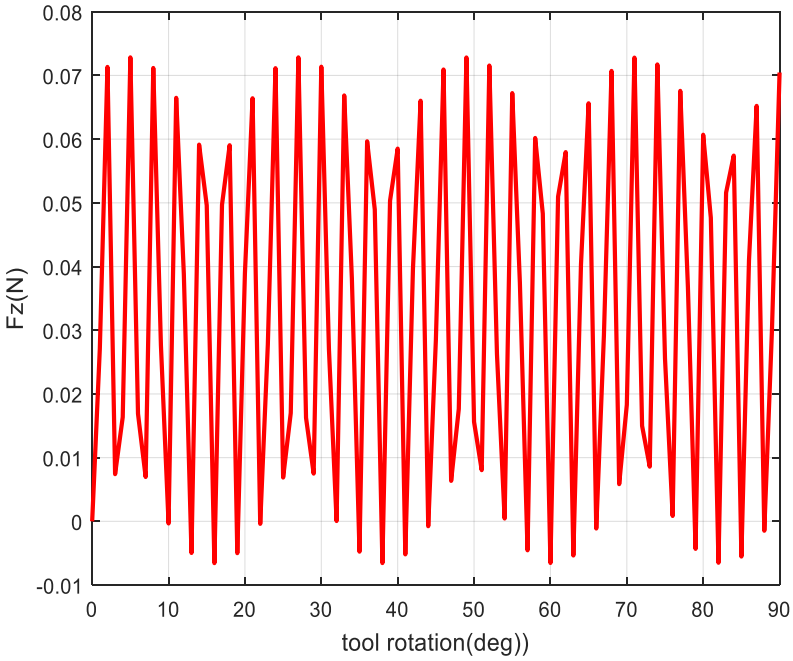

Fig. 6d. Force variation in axial direction for 270º - 360º

The force variation in the axial direction follows a sinusoidal function of repeated pattern but the cutter experience different magnitude of force in a cycle of cut as the tool direction changes. The force increases as the tool rotation angle increases on the axial direction. Also, it is depicted from the analysis that the helix angle as the geometric compliment of the tool rotation angle and has a sensitive effect on the micro-cutting process. The helix angle determines the power, surface finish and the efficiency of cutting process. The former is also material sensitive and therefore there are preferred helix angle for different material to undergo cutting process. The higher the axial force the higher the axial force exerted by the tool on the holder and lesser the radial vibration of the tool and vice versa. The force exerted on the micro-cutter increases as the tool rotation angle increases in the feed direction.

The material considered in this research paper is an aluminum alloy AlT0061 which have its use extensively in the aerospace sector and naturally because of the high structural rigidity involved in the application of the material in this field of manufacturing, the helix angle 45º is the preferred selection as the micro-cutter experiences average force to machine this component. The force exerted on the micro-cutter increases as the tool rotation angle increases in normal axial direction.

The micro-cutter experiences reduced force on this axis of rotation because it is the normal to the feed direction. For AlT0061 the tool helix angle 45 degrees is preferred because of the rigidity of the material of cut. At the axial direction the tool experiences more of the negative deflection of the force which means that as the tool helix angle increases the tool experience more axial force against the tool holder and lesser axial force in the direction of the material that is in cut. The same way in conventional cutting process increase in the tool angle increases the magnitude of the force felt in axial direction but lesser radial vibration.

4. 4. The linear tool dynamics: vibration behavior in the feed direction

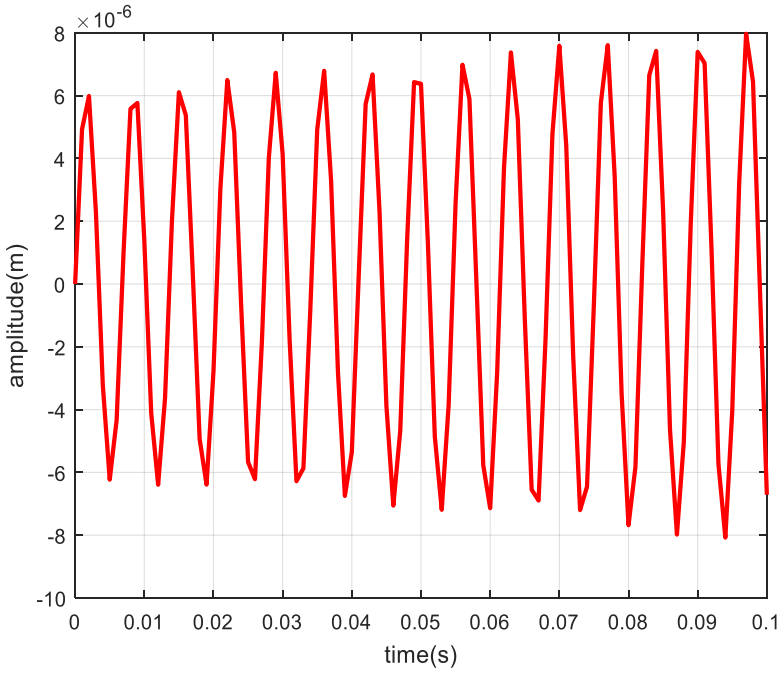

Fig. 7a. Displacement in feed direction for t = 0 - 0.1s

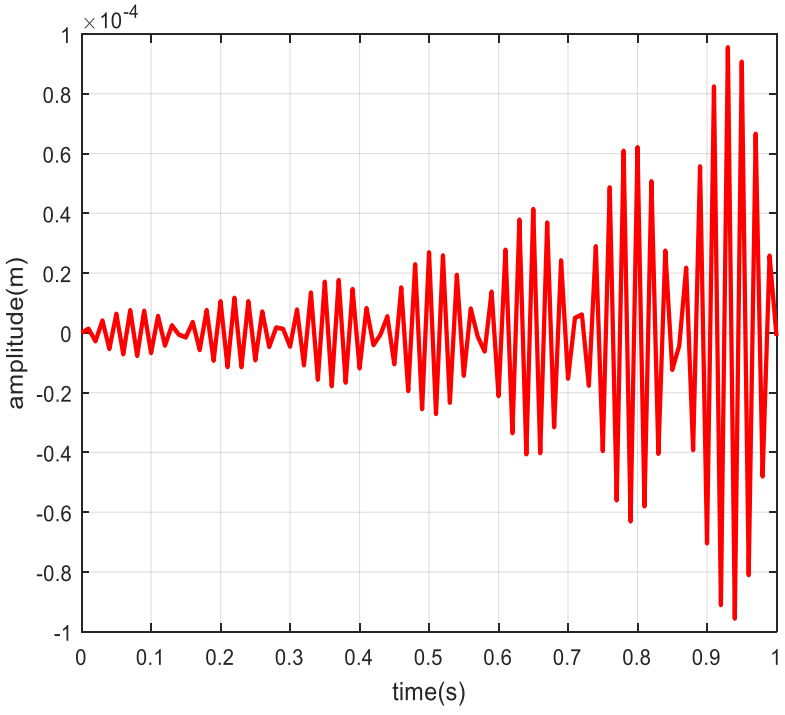

Fig. 7b. Displacement in feed direction for t = 0 - 1s

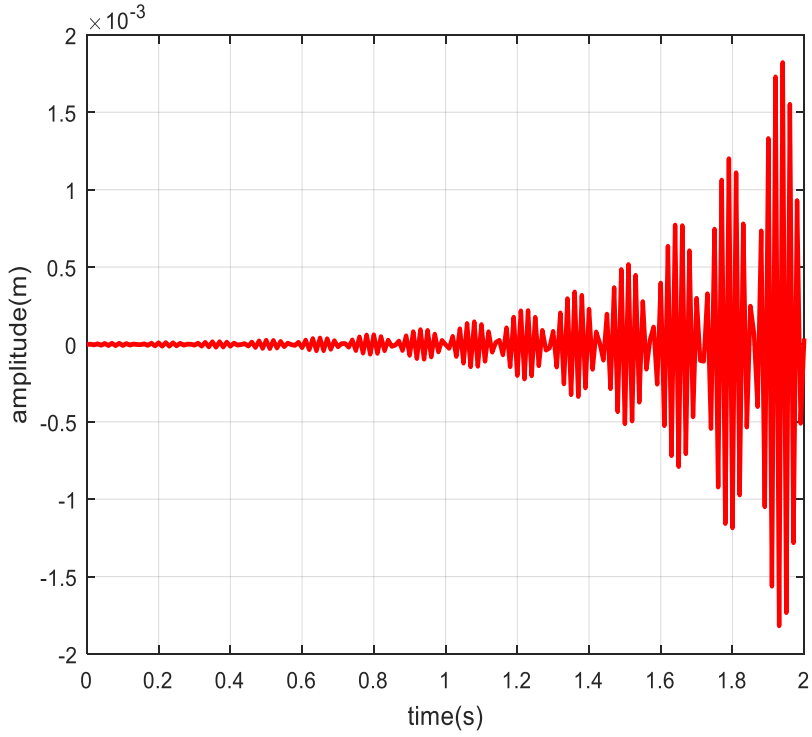

Fig. 7c. Displacement in feed direction for t = 0 - 2s

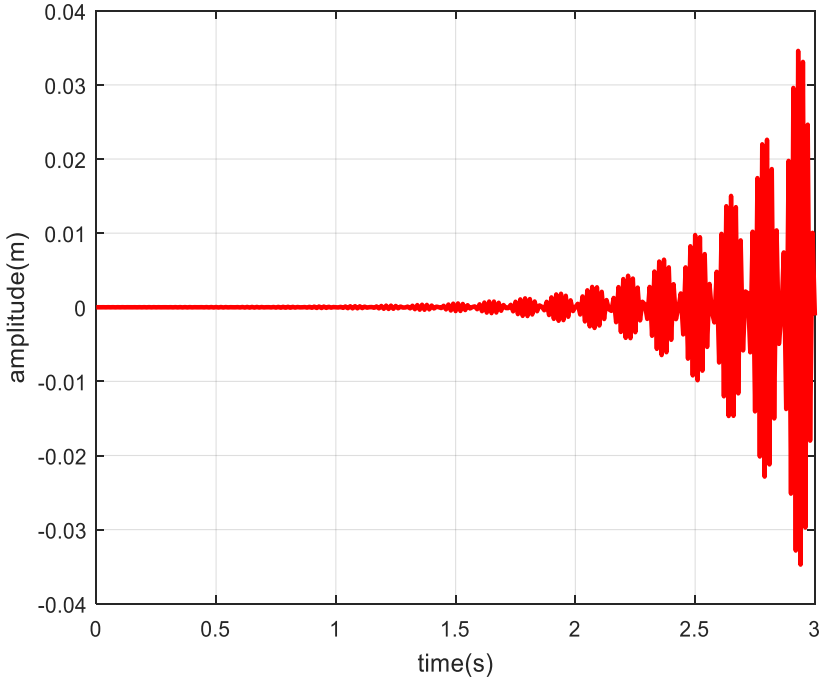

Fig. 7d. Displacement in feed direction for t = 0 - 3s

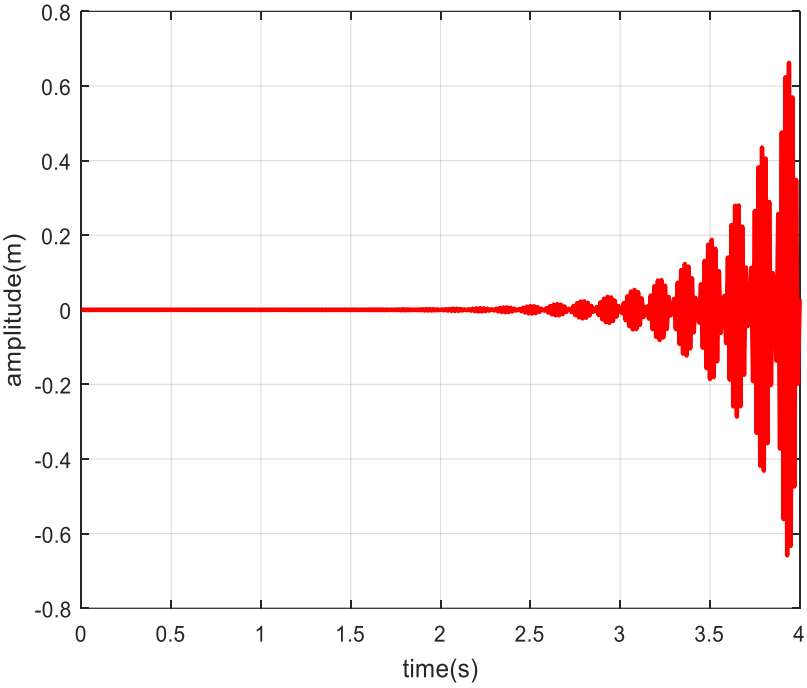

Fig. 7e. Displacement in feed direction for t = 0 - 4s

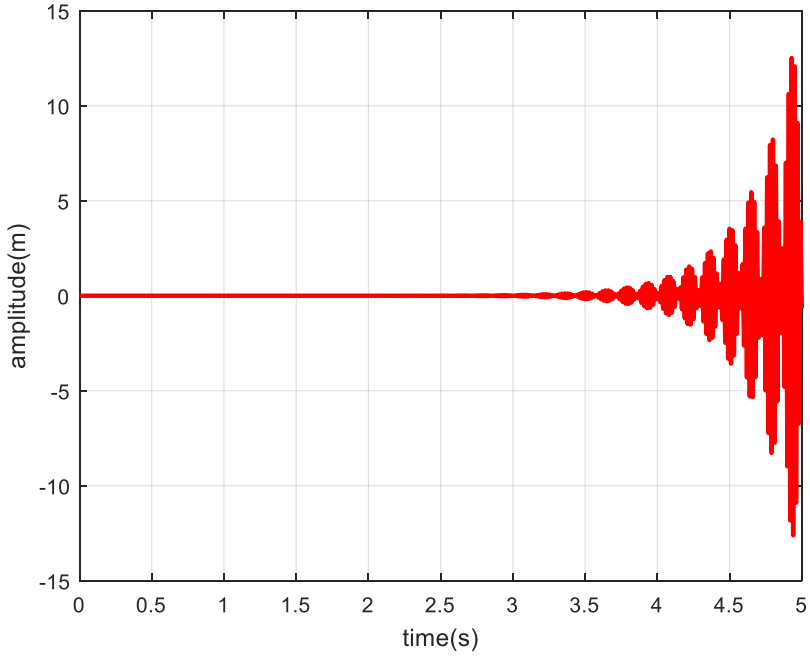

Fig. 7f. Displacement in feed direction for t = 0 - 5s

4. 5. The linear tool dynamics: vibration behavior in the opposite feed direction

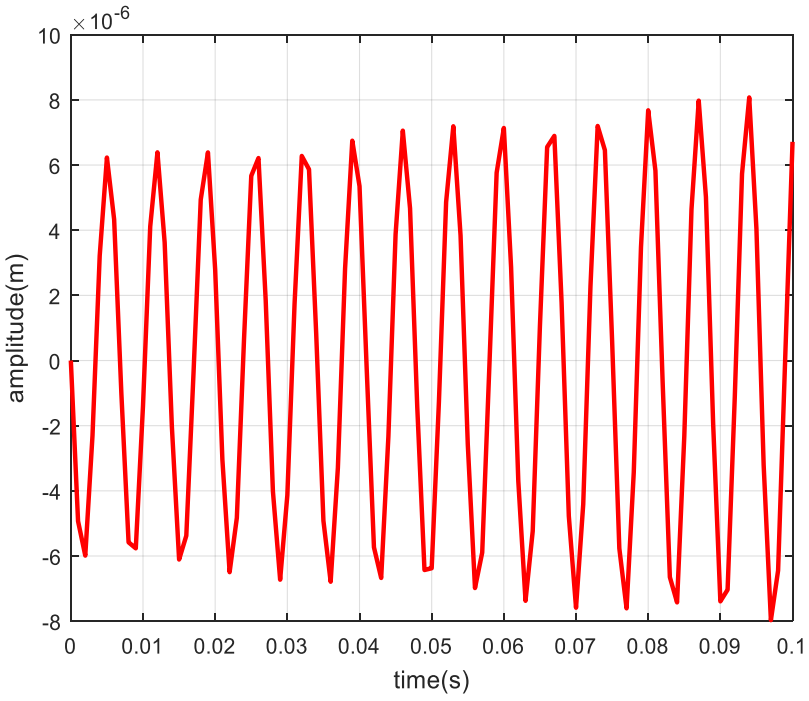

Fig. 8a. Displacement in feed direction for t = 0 - 0.1s

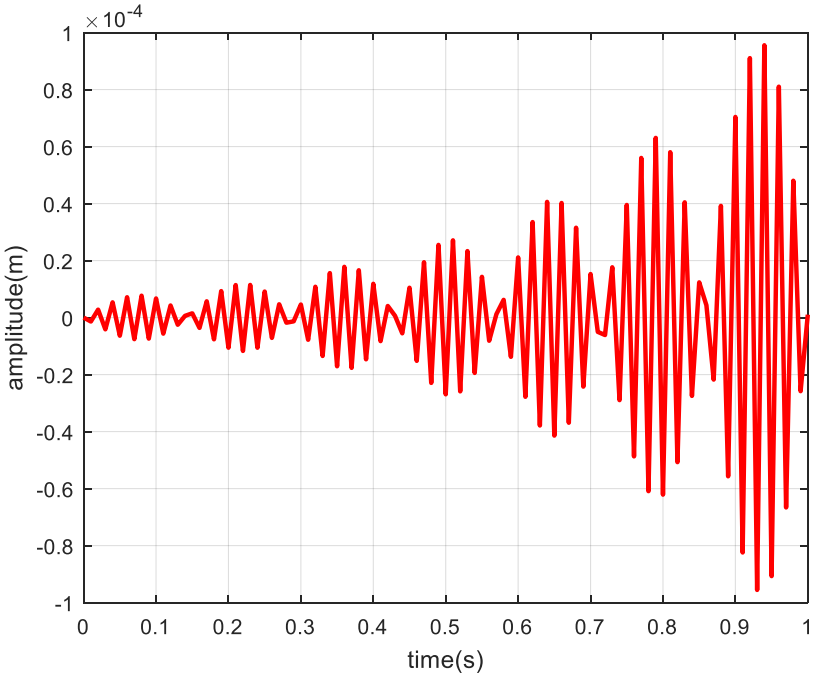

Fig. 8b. Displacement in feed direction for t = 0 - 1s

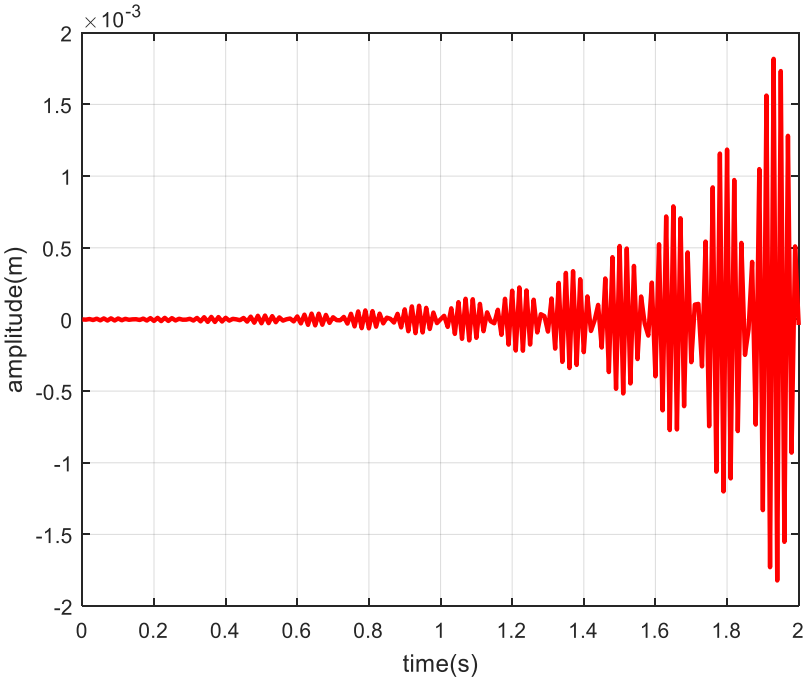

Fig. 8c. Displacement in feed direction for t = 0 - 2s

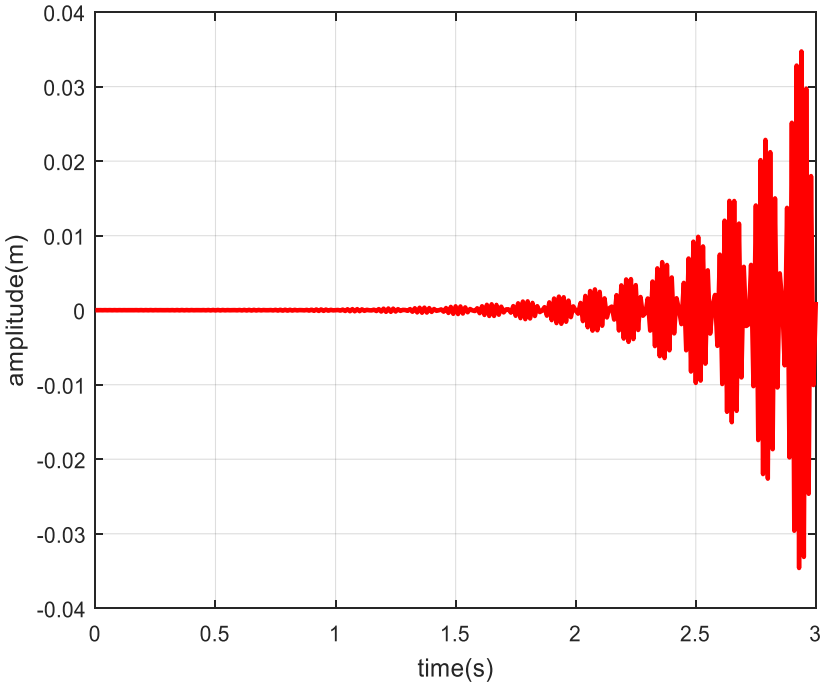

Fig. 8d. Displacement in feed direction for t = 0 - 3s

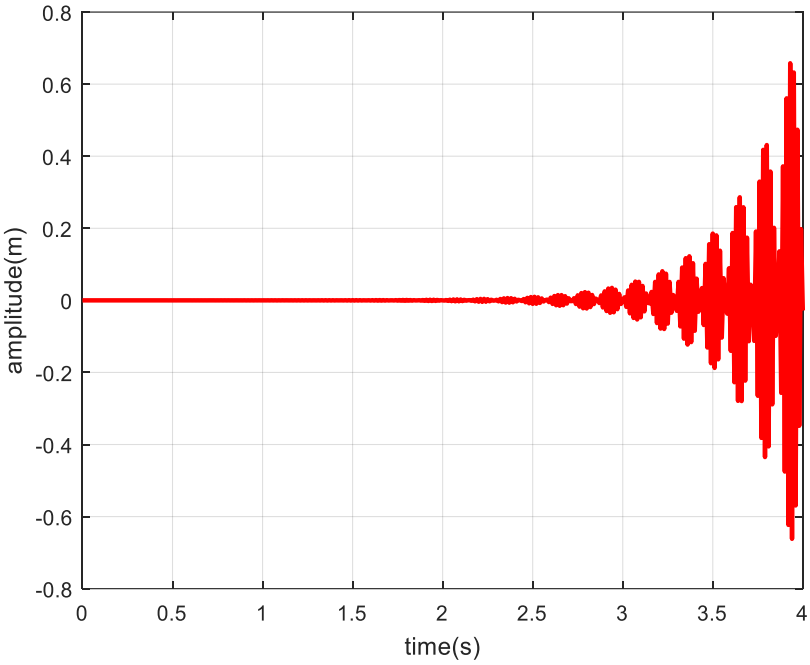

Fig. 8e. Displacement in feed direction for t = 0 - 4s

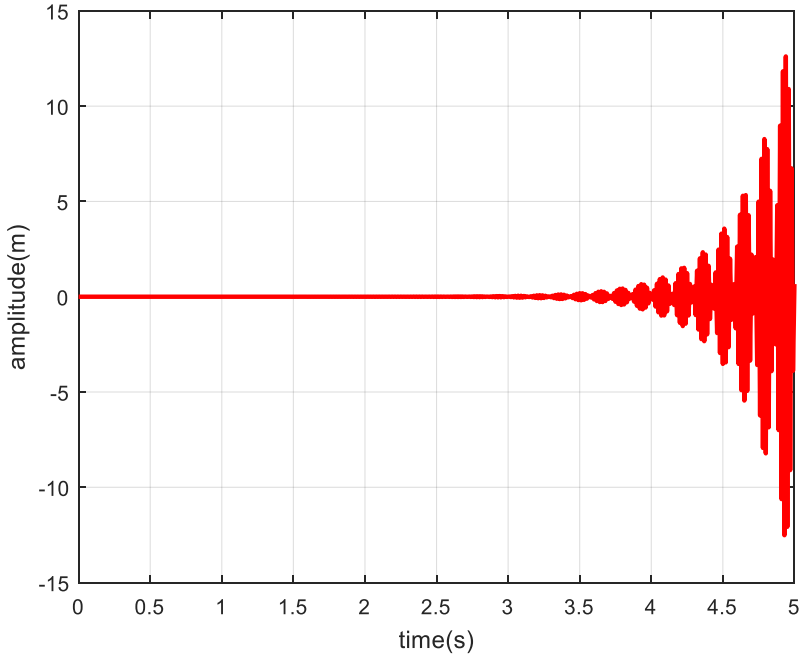

Fig. 8f. Displacement in feed direction for t = 0 - 5s

4. 6. The linear tool dynamics: Actual vibration behavior in the feed direction

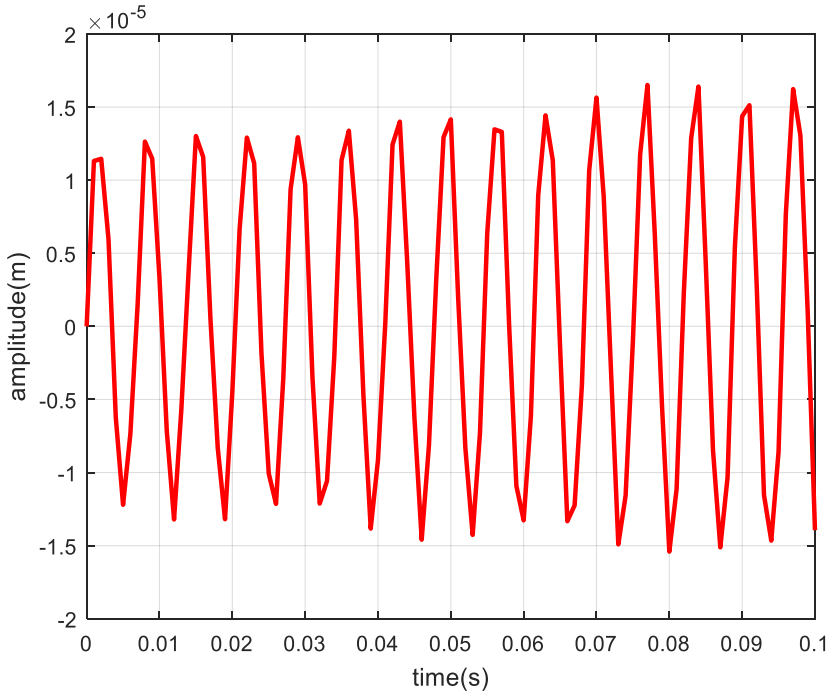

Fig. 9a. Displacement in feed direction for t = 0 - 0.1s

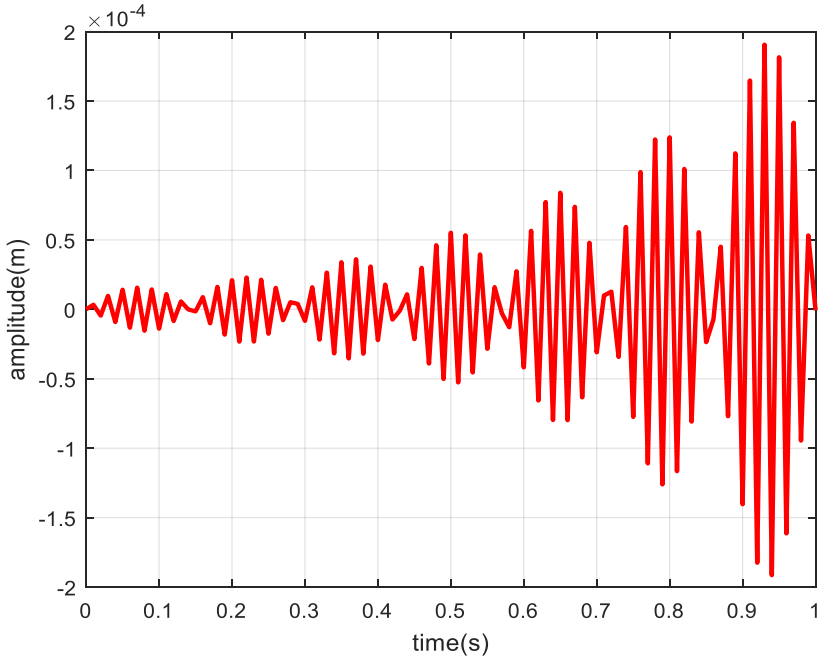

Fig. 9b. Displacement in feed direction for t = 0 - 1s

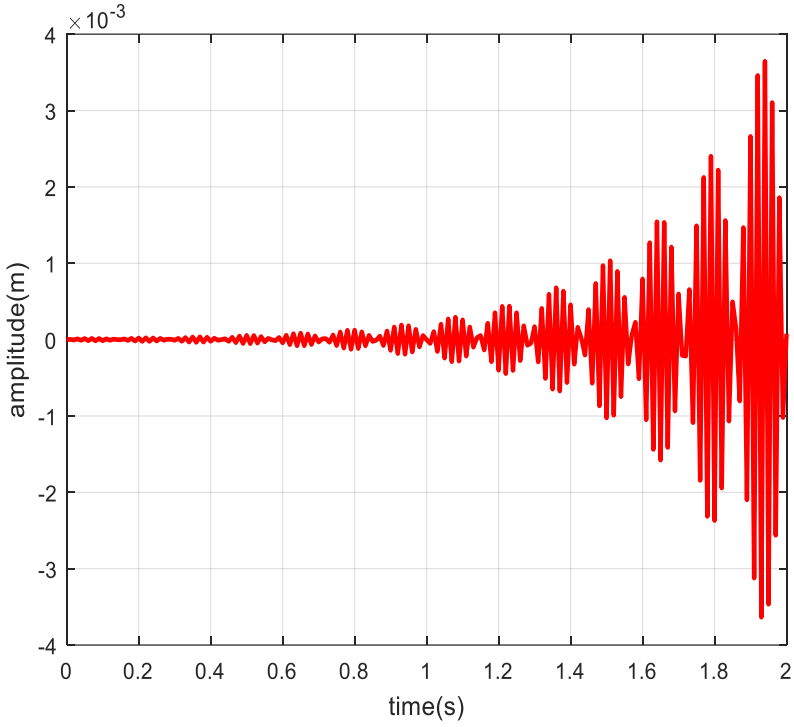

Fig. 9c. Displacement in feed direction for t = 0 - 2s

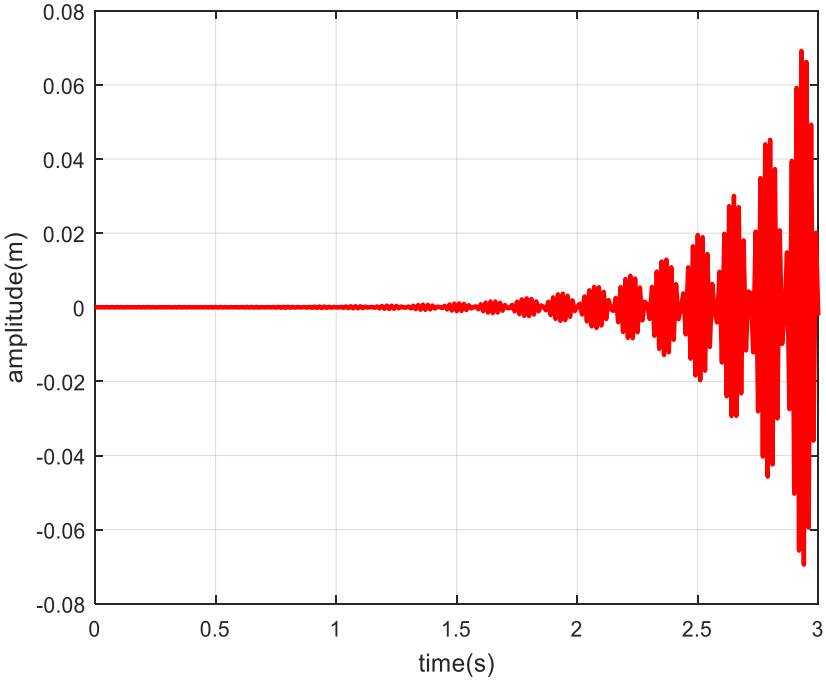

Fig. 9d. Displacement in feed direction for t = 0 - 3s

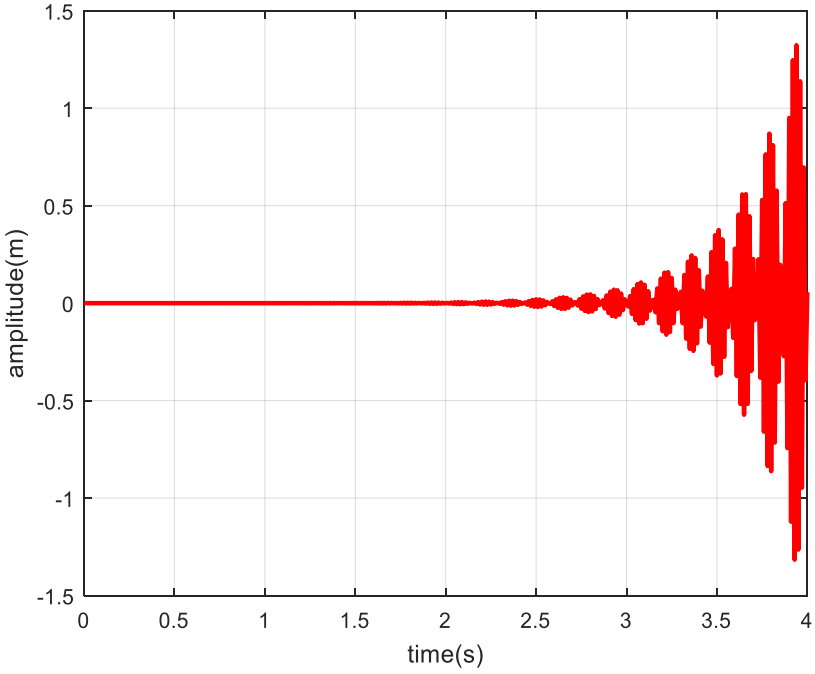

Fig. 9e. Displacement in feed direction for t = 0 - 4s

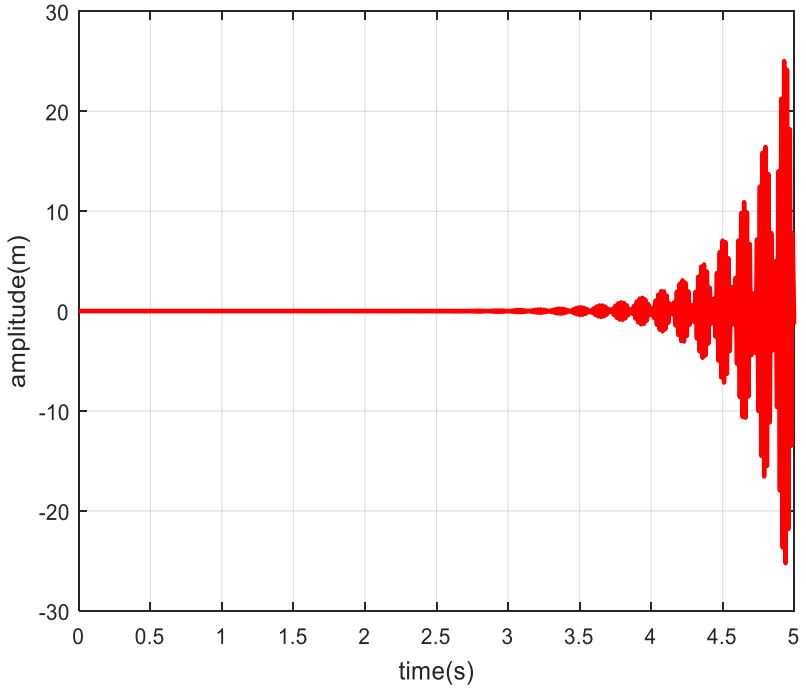

Fig. 9f. Displacement in feed direction for t = 0 - 5s

Fig. 7a-e illustrate the vibration of the system in the feed direction while Fig. 8a-e depict simulation of the vibratory behaviour of the system in the opposite feed direction. Also, Fig. 9a-e presented the actual vibration on the feed direction as a relative difference between the former and hence the amplitude of vibration increased. The figures show that the amplitude of vibration increases with increase depth of cut which supports machine tool theory.

4. 7. The linear tool dynamics: vibration behavior in the normal direction

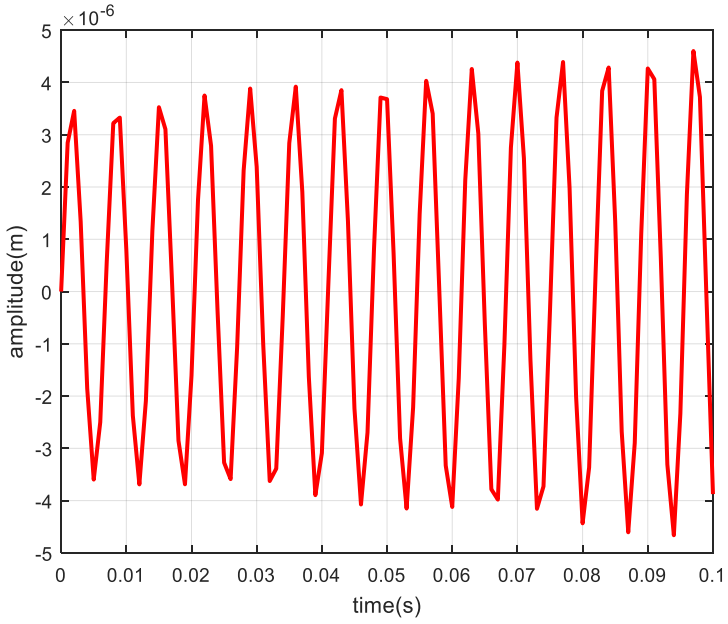

Fig. 10a. Displacement in feed direction for t = 0 - 0.1s

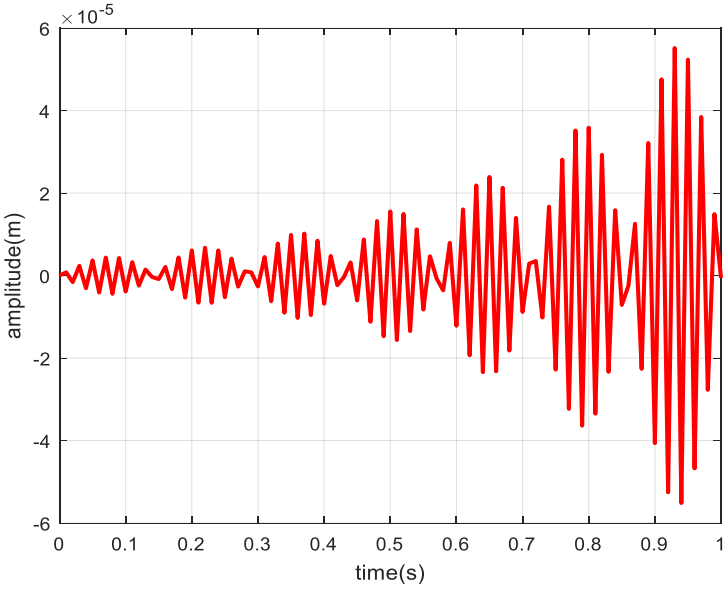

Fig. 10b. Displacement in feed direction for t = 0 - 1s

Fig. 10a-e shows the dynamic behaviour of the system in the normal direction to the feed. It is nearly the same except with little differnces. This shows the milling cutter experiences nearly the same vibration in both direction on the normal axis. The actual vibration experienced on the micro-cutter is lower than the one experienced on the feed direction. This is actually what is expected as the normal direction do not offer any resistance to the feed direction.

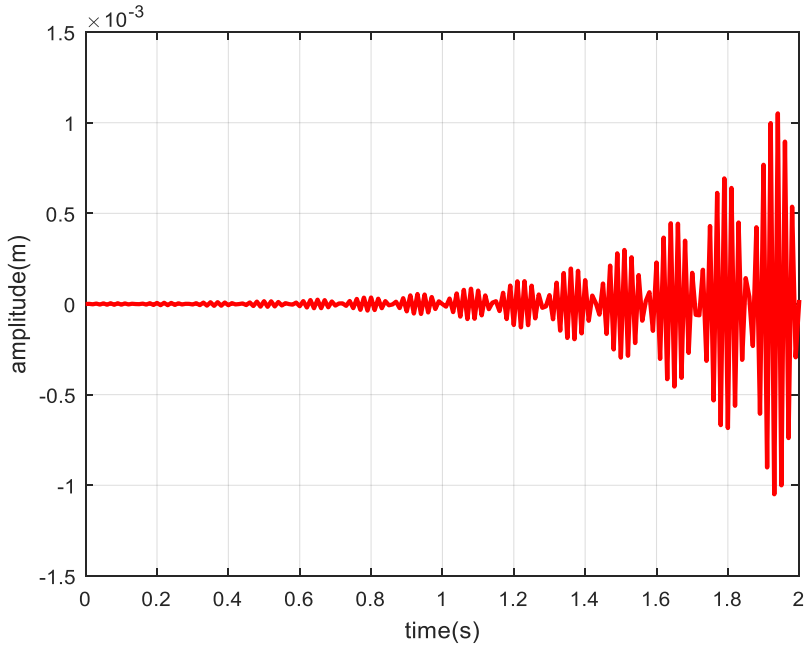

Fig. 10c. Displacement in feed direction for t = 0 - 2s

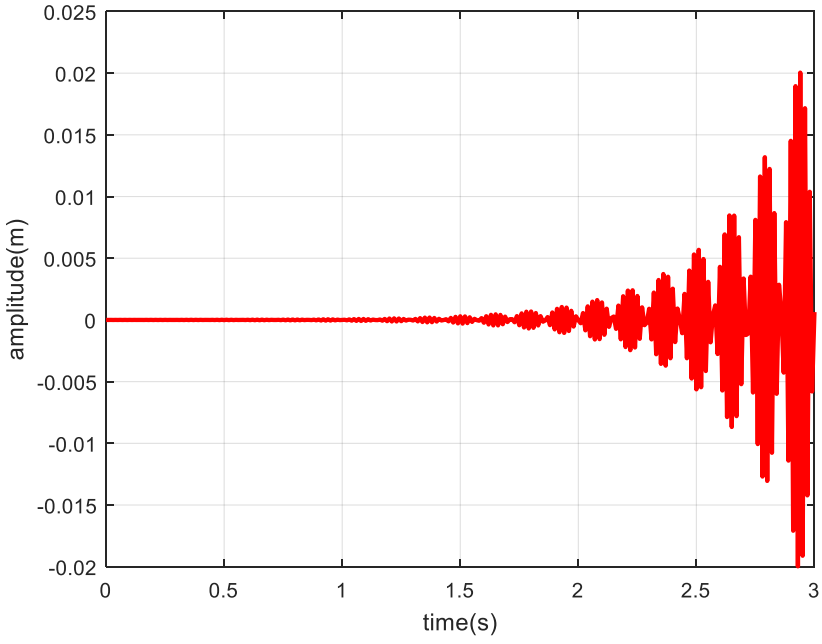

Fig. 10d. Displacement in feed direction for t = 0 - 3s

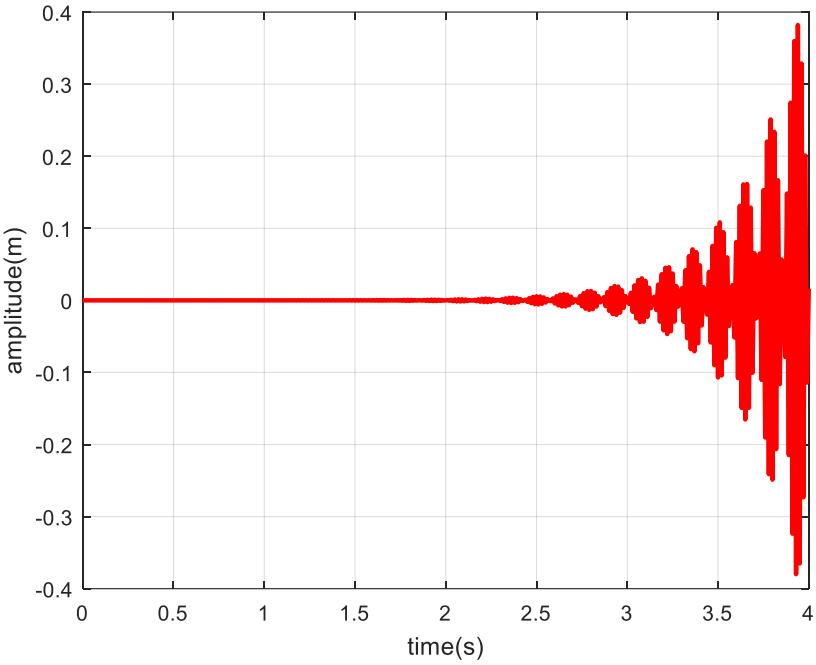

Fig. 10e. Displacement in feed direction for t = 0 - 0.1s

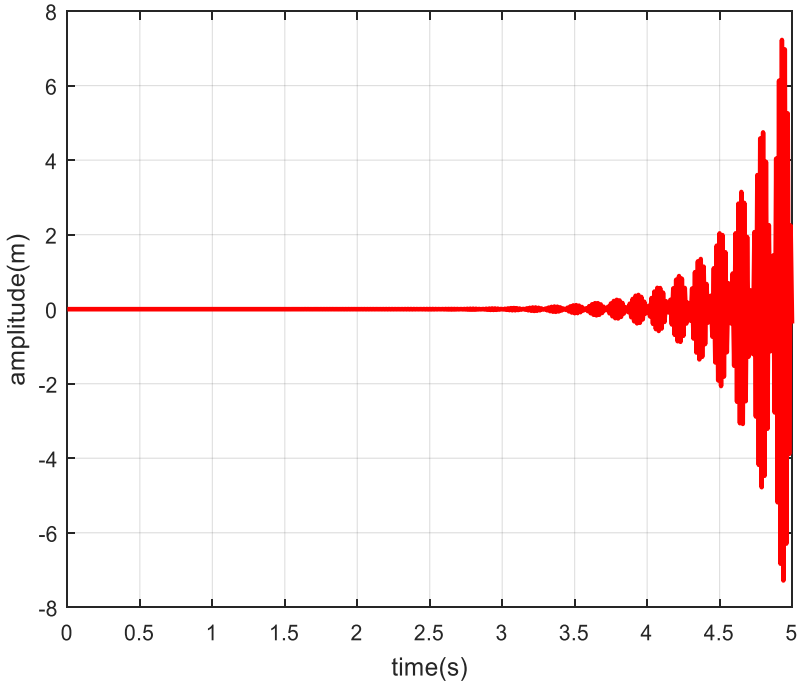

Fig. 10f. Displacement in feed direction for t = 0 - 1s

4. 8. The nonlinear tool dynamics: vibration behavior in the feed direction

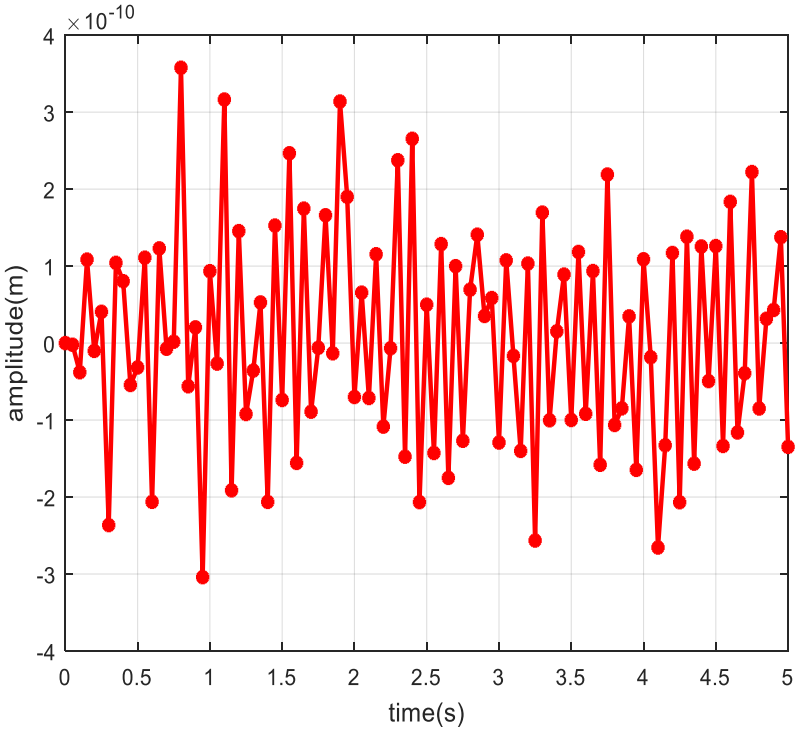

Fig. 11. Displacement in feed direction

Fig. 11 shows the nonlinear behaviour of the tool in the feed direction. The response is true vibratory response of the system that has amplitude stability due to the nonlinearity introduced in the structural dynamics as the hysteretic damping. The hysteretic damping makes the vibration experienced by the tool not go beyond the micro-scale level because the system balances itself through internal damping of excess vibrations The milling cutter in vibration assisted micro-end milling experiences a balanced displacement provided the appropriate feed rate is selected.

The system exhibits finite amplitude stability as the amplitude of vibration on this axis of cut is on the micro-scale. The amplitude of vibration is maximum when compared to other axis of cut which is due to the fact that the axis is opposite the feed direction.

4. 9. The nonlinear tool dynamics: vibration behavior in the normal and axial directions

Fig. 12 shows the simulated vibration behavior on the normal axis of rotation. Amplitude stability is also maintained due to non-linearity introduced by the hysteretic damping. The maximum amplitude of rotation experienced is lower than that experienced in the feed direction. The amplitude is stabilized to the scale of cut to any time of cut. The same behaviour is experienced in vibration behavior on the normal axis of rotation as depicted in Fig. 13.

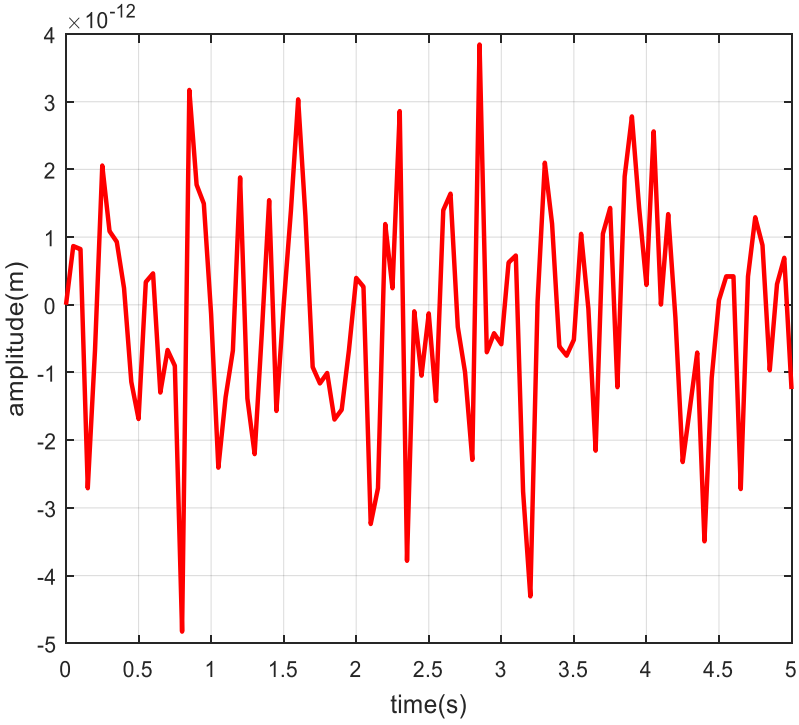

Fig. 12. Displacement in normal direction

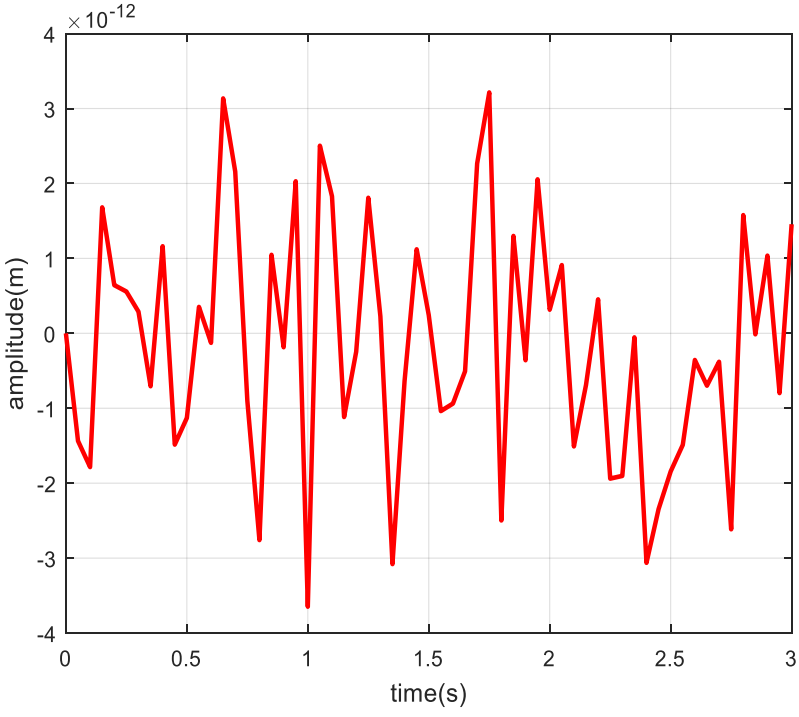

Fig. 13. Displacement in axial direction

5. CONCLUSIONS

In this work, force as well as linear and nonlinear phenomena of chatter that occurs in the tool and the work piece during vibration assisted micro-milling processes have been modelled and analyzed. The obtained analytical solutions were used to determine the stability region of the machining processes involved. With the aid of the developed solutions, parametric studies were carried out. Also, the results show satisfactory agreement with earlier works

Nomenclature

h	Chip thickness	(μm)
η	axial depth	(μm)
R_e	Edge radius	(μm)
h_m	Minimum chip thickness	(μm)
V_H	Vickers hardness parameter	
f	feed rate	(μm/s)
F_z	feedpertooth	(μm/tooth)
c_1	Experimental constant	
c_2	Experimental constant	
E	Elastic Modulus	(Pa)
b	width of cut	(μm)
Y	Yield Strength	(N/mm^2)
σ	Flow stress	
r	The tool radius	(μm)
θ_f	Relief angle	(°)
β	Tool helix angle	(°)
θ	Tool rotation angle	(°)
f	Shear angle	(°)
f_x	Phase angle in x-direction	(°)
f_y	Phase angle in y-direction	(°)
N	Number of teeth	
k	Ordinal number of tool teeth	
t	Time	(s)
ω_n	Natural frequency	()
J	Experimental constant	
ω	Palstance	(rad/s)
γ_1	Experimental constant	
γ_2	Experimental constant	

References

[1] M. Xiao, S. Karube, T. Soutome, K. Sato. Analysis of chatter suppression in vibration cutting. *International Journal of Machine Tools and Manufacture*, 42(15) (2002) 1677-1685

[2] S. M. K Tabatabaei, S. Behbahani and S.M. Mirian, Analysis of ultrasonic assisted machining (UAM) on regenerative chatter in turning. *Journal of Materials Processing Technology*, 213(3) (2013) 418-425

[3] W.Y. Bao, I. N. Tansel. Modeling micro-end-milling operations. Part I: analytical cutting force model. *Int. J. Mach. T. Manuf.* V 40 (2000) 2155-2173

[4] X. Fan and M. H. Miller. Force Modeling in Vibration Assisted Cutting. Proc. of the 2001 ASPE Annual Meeting, 409-412.

[5] T. A. Dow, M. A. Cerniway and A. Sohn. Vibration Assisted Diamond Turning Using Elliptical Tool Motion. Proc. of the 2001 ASPE Annual Meeting, 92-97.

[6] N. H. Hanna and Tobias, S. A. A theory of nonlinear regenerative chatter. *Trans. ASME, J. Engng Ind.* 96 (1974) 247-255

[7] Y. Altintas and E. Budak. Analytical prediction of stability lobes in milling. *Ann. CIRP*, 44(1) (1995) 357-362

[8] E. Budak and Y. Altintas. Analytical prediction of chatter stability in milling, Part I: general formulation. *Trans. ASME, J. Dyn. Syst. Meas. Control* 120(1) (1998) 22-30

[9] E. Budak and Y. Altintas. Analytical prediction of chatter stability in milling, Part II: application of the general formulation to common milling systems.*Trans. ASME, J. Dyn. Syst. Meas. Control* 120(1) (1998) 31-36

[10] X. K. Luo, K. Cheng, K., X. C. Luo and X. V. Liu, X. W. A simulated investigation on the machining instability and dynamic surface generation. *Int. J. Adv. Mf. Technol.* 26 (2005) 457-465

[11] F. Vollertsen, D. Biermann, H. N. Hansen, I. S. Jawahir, K. Kuzman. Size effects in manufacturing of metallic components. *CIRP Annals*, V 58 (2009) 566-587

[12] V. I. Babitsky, A. N. Kalashnikov, A. Meadows, and A. A. H. P. Wijesundara. Ultrasonically assisted turning of aviation materials. *J. Mater. Process. Technol.* 132 (2003) 157-160

[13] H. Jamshidi, M.J. Nategh, Theoretical and experimental investigation of the frictional behavior of the tool–chip interface in ultrasonic vibration assisted turning. *Int. J. Mach. Tools Manuf.* 65 (2013) 1-7.

[14] S. Patil, S. Joshi, A. Tewari, S.S. Joshi, Modelling and simulation of effect of ultrasonic vibrations on machining of Ti6Al4V. *Ultrason.* 54 (2014) 694-705

[15] P. Guo, K.F. Ehmann, An analysis of the surface generation mechanics of the elliptical vibration texturing process. *Int. J. Mach. Tools Manuf.* 64 (2013) 85-95

[16] Ahmed Syed Adnan, Sathyan Subbiah. Experimental investigation of transverse vibration-assisted orthogonal cutting of AL-2024. *International Journal of Machine Tools and Manufacture* Volume 50, Issue 3, March 2010, Pages 294-302

[17] Maroju Naresh Kumar, S. Kanmani Subbu, P. Vamsi Krishna, A. Venugopal. Vibration Assisted Conventional and Advanced Machining: A Review. *Procedia Engineering* Volume 97, 2014, Pages 1577-1586

[18] X. Zhang, A.S. Kumar, M. Rahman, C. Nath, K. Liu, Experimental study on ultrasonic elliptical vibration cutting of hardened steel using PCD tools. *J. Mater. Process. Technol.* 211 (2011) 1701-1709

[19] J.C. Outeiroa, J.P. Costesa, J.R. Kornmeierb. Cyclic variation of residual stress induced by tool vibration in machining operations. *Procedia CIRP*. 8 (2013) 493-497

[20] H. Ding, R. Ibrahim, K. Cheng, S.-J. Chena, Experimental study on machinability improvement of hardened tool steel using two-dimensional vibration-assisted micro-end-milling. *Int. J. Mach. Tools Manuf.* 50 (2010) 1115-1118

[21] X.-H. Shen, J.-H. Zhang, H. Li, J.-J. Wang, X.-C. Wang, Ultrasonic vibration-assisted milling of aluminum alloy. *Int. J. Adv. Manuf. Technol.* 63 (2012) 41-49

[22] H. Liana, Z. Guoa, Z. Huanga, Y. Tanga, J. Songa, Experimental research of Al-6061 on ultrasonic vibration assisted micro-milling. *Procedia CIRP*. 6 (2013) 561-564

[23] S.S.F. Chang, G.M. Bone. Thrust force model for vibration assisted drilling of aluminum 6061-T6. *Int. J. Mach. Tools Manuf.* 49 (2009) 1070-1076

[24] V.A. Phadnis, A. Roy, V.V. Silberschmidt, A finite element model of ultrasonically assisted drilling in carbon/epoxy composites. *Procedia CIRP*. 8 (2013) 141-146

[25] M.A. Kadivar, J. Akbari, R. Yousefi, A. Rahi, M. Ghahramani Nick, Investigating the effects of vibration method on ultrasonic-assisted drilling of Al/Sicp metal matrix composites. *Rob. Comput. Integr. Manuf.* 30 (2014) 344-350

[26] M. Aziza, O. Ohnishib, H. Onikurab, Novel micro deep drilling using micro long flat drill with ultrasonic vibration. *Precis. Eng.* 36 (2012) 168-174

[27] P. Mehbudia, V. Baghlania, J. Akbaria, A.R. Bushroab, N.A. Mardib, Applying ultrasonic vibration to decrease drilling-induced delamination in GFRP laminates. *Procedia CIRP* 6 (2013) 577-582

[28] S. Aoki, S. Hirai, T. Nishimura, Prevention from delamination of compositematerial during drilling using ultrasonic vibration. *Key Eng. Mater.* 291-292 (2005) 465-470

[29] Z. Liang, Y. Wub, X. Wanga, A new two-dimensional ultrasonic assisted grinding (2D-UAG) method and its fundamental performance in mono crystal silicon machining. *Int. J. Mach. Tools Manuf.* 50 (2010) 728-736

[30] G. Chern and Y. Chang. Using two-dimensional vibration cutting for micro-milling. *Int. J. Mach. Tools Mf.* 46 (2006) 659-666

[31] I. S. Kang, J. S. Kim, J. H. Kim, M. C. Kang, and Y. W. Seo. A mechanis tic model of cutting force in the micro end milling process. *J. Mater. Process. Technol.* 187-188 (2007) 250-255

[32] M. T. Zaman, S. Kumar, A., M. Rahman, and S. Sreeram. A three-dimensional analytical cutting force model for micro end milling operation. *Int. J. Mach. Tools Mf.* 46 (2006) 353-366

[33] H. Ding, S. Chen and K. Cheng Two dimensional vibration-assisted micro-milling: kinematics simulation, chip thickness computation and analysis. *Adv. Mater. Res.* 97-101 (2010) 2779-2784

[34] Y. Gaoa, R. Sun, J. Leopold. Analysis of cutting stability in vibration assisted machining using an analytical predictive force model. *Procedia CIRP* 31 (2015) 515-520

[35] H. Z. Li, K. Liu, X. P. Li. A new method for determining the undeformed chip thickness in milling. *J Mater Proc Technol* 113(15) (2001) 378-384

[36] Yanjie Yuan, Xiubing Jing, Kornel F. Ehmann, Jian Cao, Huaizhong Li, Dawei Zhang. Modeling of cutting forces in micro end-milling. *Journal of Manufacturing Processes* Volume 31, January 2018, Pages 844-858